AD_____

Award Number: DAMD17-00-1-0429

TITLE: Radiolabeled Herceptin to Increase Treatment Efficacy in Breast Cancer Patients With Low Tumor HER-2/neu Expression

PRINCIPAL INVESTIGATOR: George Sgouros, Ph.D.

CONTRACTING ORGANIZATION: Sloan-Kettering Institute
for Cancer Research
New York, New York 10021

REPORT DATE: July 2001

TYPE OF REPORT: Annual

PREPARED FOR: U.S. Army Medical Research and Materiel Command
Fort Detrick, Maryland 21702-5012

REPORT DOCUMENTATION PAGE

Form Approved
OMB No. 074-0188

1. AGENCY USE ONLY (Leave blank)	2. REPORT DATE	3. REPORT TYPE AND DATES COVERED
	July 2001	Annual (15 Jun 00 - 14 Jun 01)

4. TITLE AND SUBTITLE

Radiolabeled Herceptin to Increase Treatment Efficacy in Breast Cancer Patients With Low Tumor HER-2/neu Expression

5. FUNDING NUMBERS

DAMD17-00-1-0429

6. AUTHOR(S)

George Sgouros, Ph.D.

7. PERFORMING ORGANIZATION NAME(S) AND ADDRESS(ES)

Sloan-Kettering Institute
for Cancer Research
New York, New York 10021
E-Mail:sgourosg@mskcc.org

8. PERFORMING ORGANIZATION REPORT NUMBER

9. SPONSORING / MONITORING AGENCY NAME(S) AND ADDRESS(ES)

U.S. Army Medical Research and Materiel Command
Fort Detrick, Maryland 21702-5012

10. SPONSORING / MONITORING AGENCY REPORT NUMBER

11. SUPPLEMENTARY NOTES

Report contains color

20011130 060

12a. DISTRIBUTION / AVAILABILITY STATEMENT

Approved for Public Release; Distribution Unlimited

12b. DISTRIBUTION CODE

13. ABSTRACT *(Maximum 200 Words)*

The primary objective of the proposal is to evaluate the efficacy and feasibility of using radiolabeled Herceptin antibody to target rapidly accessible breast carcinoma cells or micrometastases. By using Herceptin to specifically deliver radiation we anticipate that the efficacy of Herceptin will be extended to include breast cancer cells that are not high HER-2/neu antigen expressors. This hypothesis will be tested using the spheroid model to simulate rapidly accessible micrometastases. An alpha-particle emitting radionuclide will be used to enhance tumor cell kill. Spheroids of 3 breast carcinoma cell lines exhibiting, high, intermediate and low expression of HER-2/neu have been generated and characterized (task 1). Antibody penetration by confocal microscopy has been measured for these 3 spheroids and an appropriate Herceptin concentration has been chosen for cell kill experiments (task 2). Preliminary cell kill experiments using Herceptin labeled with an alpha-particle emitter have been carried out; dose-response studies have been started and are on going (task 3: month 7-20). Preliminary results suggest that alpha-emitter labeled Herceptin will be effective against tumor cells that have a 3 to 4-fold lower expression of HER2/neu.

14. SUBJECT TERMS	15. NUMBER OF PAGES
Herceptin, HER-2/neu, alpha particle emitters, Ac-225, micrometastases	32
	16. PRICE CODE

17. SECURITY CLASSIFICATION OF REPORT	18. SECURITY CLASSIFICATION OF THIS PAGE	19. SECURITY CLASSIFICATION OF ABSTRACT	20. LIMITATION OF ABSTRACT
Unclassified	Unclassified	Unclassified	Unlimited

Table of Contents

INTRODUCTION

In combination with chemotherapy, the antitumor activity of Herceptin (anti-Her-2/neu), a humanized monoclonal antibody directed against HER-2/neu, has been effective in treatment of breast cancer cells overexpressing HER-2/neu. This promising, FDA approved, and commercially available antibody may be effective in eradicating pre-vascularized micormetastatic disease when labeled with a short lived alpha particle emitter. Alpha particles are very effective in sterilizing cells, and 1 to 3 particles transversing the cell is enough for cell kill. Therefore, this treatment approach may have the potential of eradicating micrometastatic disease both of non-overexpressing and overexpressing breast cancer cells. These hypotheses will be tested first on a tumor spheroid model that can be closely controlled. Spheroids of breast cancer cells expressing different levels of HER-2/neu will be incubated with Herceptin labeled with an alpha particle emitting radionuclide. This model will be used to determine optimal antibody concentration, dose level and treatment schedule. Using the results obtained from the *in vitro* spheroid system, a pilot effort to obtain preliminary data on treatment response *in vivo* will be undertaken. Spheroids will be injected intraperitoneally in athymic mice and response to Bi-213-Herceptin therapy will be monitored using MR imaging. The cells in the injected spheroids will be tagged with a MRI contrast agent. The potential of Dexamethasone to enhance radiosensitivity by increased apoptotic death will be examined. The proposed study may result in a novel treatment approach where Herceptin will be used to eradicate breast cancer micrometastases expressing HER-2/neu.

BODY

Task 1 (month 1-3) - Make spheroids of the four cell lines HBL-100, BT-474, MDA-MB-361 and MDA-MB-175-VII.

Spheroids have been generated using the cell lines, BT-474, and MDA-MB-361. These 2 cell lines express HER-2/neu at high and intermediate levels, respectively. Attempts to generate spheroids using the cell lines, HBL-100 and MDA-MB-175-VII, were unsuccessful. To complete the range of HER-2/neu expressing spheroids, spheroids of the breast carcinoma cell line MCF7 were used to represent a low HER-2/neu expressing system.

Characterization of HER-2/neu expression

The differential HER-2/neu expression of these 3 cell lines was confirmed by flow cytometry (FACS output included in the appendix). The relative HER-2/neu expression ratios for MCF7:MDA-MB-361:BT474 are 1:4:15.

Growth characterization

The median of 24 individual spheroid growth curves for the three cell lines are depicted in figure 1. After initiation in liquid overlay culture (*1*), spheroids were placed in individual wells of a 24-well plate and spheroid growth was monitored by measuring major and minor diameters using a graduated eye-piece on an inverted optical microscope. Details are described in reference (*2*). The high HER-2/neu expressing line, BT-474, was found to grow in an unusual pattern. Over the first 10 to 20 days, the volume of untreated BT-474 spheroids decreased relative to the original spheroid volume. Beyond this initial "dip", the growth rate matched that of MCF7 spheroids. The "dip" arises because BT474 spheroids appear to undergo a 10 to 12-day period of cell shedding. Cells from the surface are shed and a core of cells remains and continues to grow leading to outgrowth of a spheroid. Our working hypothesis is that cells in the initial BT474 cell cluster are not tightly adherent to each other and that as a core of tightly adherent cells grows, the surface layer of less adherent cells is shed. Figure 2 depicts light microscope images of a typical BT474 spheroid undergoing the above-described process. The values below each image correspond to time in days. Since this dip presents difficulties in assessing the response of BT474 spheroids to Herceptin treatment, we chose to initiate BT474 spheroid experiments after the cell shedding period. Figure 3 depicts a number of BT474 spheroid control growth curves. The curve marked 1 (circles) is identical to the one in Fig. 1. The curve marked BT474-2 (diamonds) corresponds to a waiting period of approximately 7 days. Subsequent BT474 experiments (curves 3 through 5) were performed after a 20-day

Fig. 1

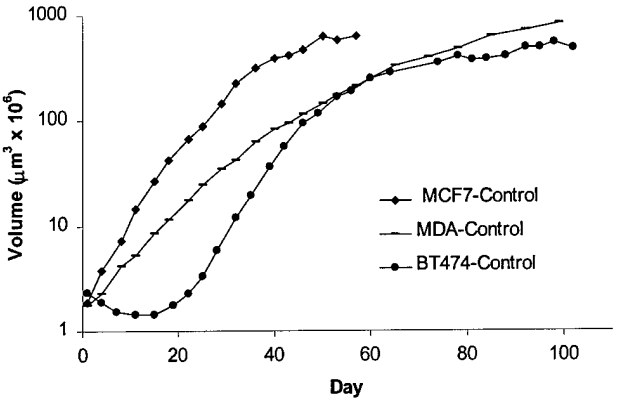

FIG 2

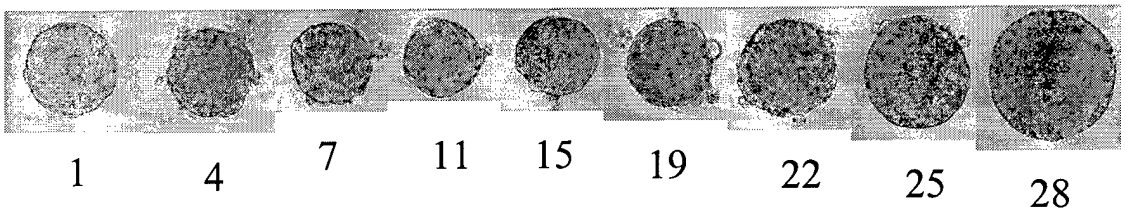

Fig. 3

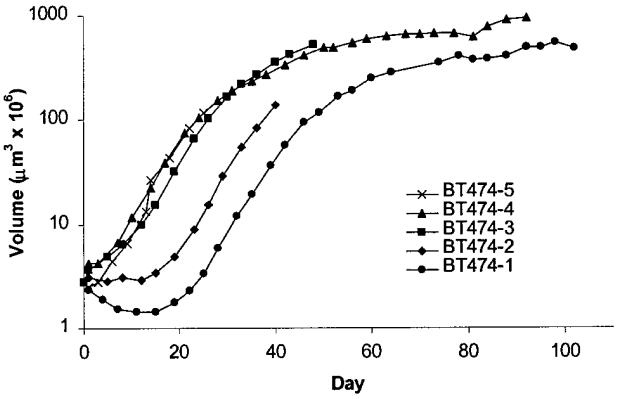

period. The figure shows good reproducibility in the control growth curve for BT474, a cell line that is known to be difficult to grow, *in vitro*.

Task 2 (month 4-6) - Characterize antibody penetration (confocal microscopy) and determine optimal Herceptin concentration for cell kill experiments in spheroids of all cell lines.

Figure 4 depicts confocal microsopy images taken through the equator of BT474 and MDA MB-361 spheroids following incubation with 10 μg/ml FITC-tagged herceptin antibody; the incubation duration is shown below each image. The images were converted to grayscale such that the green fluorescence is depicted in black. Regions that are gray or black reflect the presence of FITC-tagged Herceptin antibody. Approximately 150 to 200 μm-diameter spheroids were imaged. In the BT474 spheroids, individual cells on the spheroid rim may be clearly identified. Consistent with the known cell-surface localization of HER-2/neu, staining is seen only on the cell surface. After an incubation duration of 1, 3 or 5 hours, Herceptin has penetrated approximately 1, 2 and 3 cell layers, respectively. A similar pattern is seen with spheroids of the MDA MB-361 cell line. As expected, due to the reduced HER-2/neu expression on these cells, staining intensity is reduced. The extent of antibody peneteration, however, is similar to that seen for BT474 spheroids. These images were collected with a known concentration of FITC-

Fig. 4

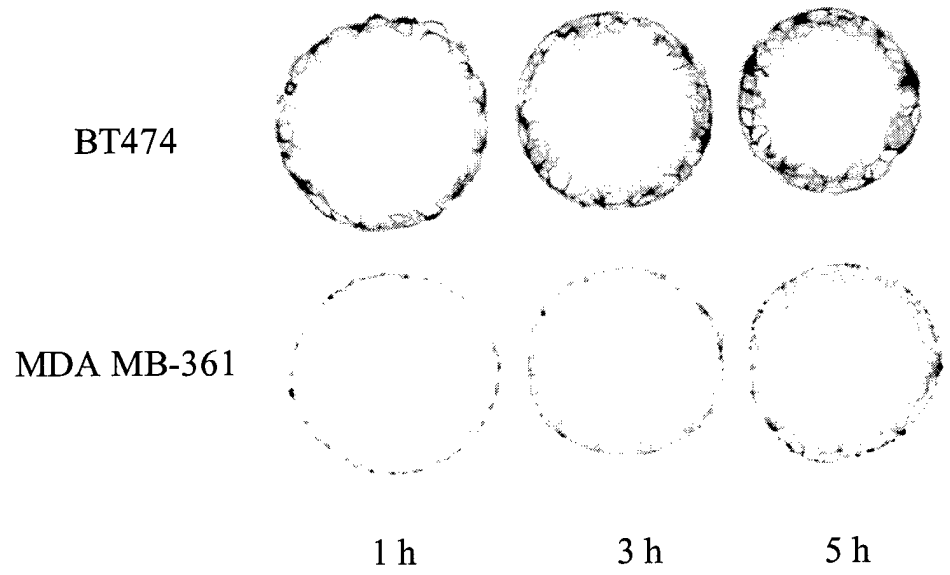

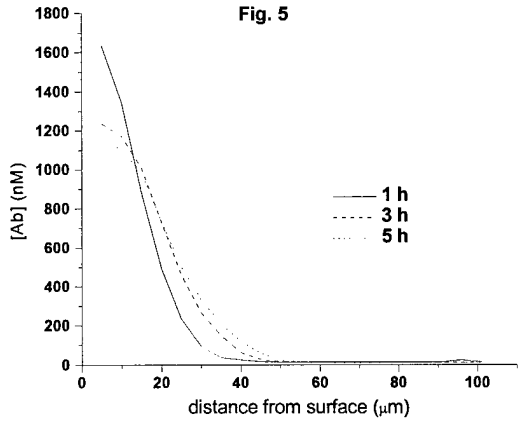

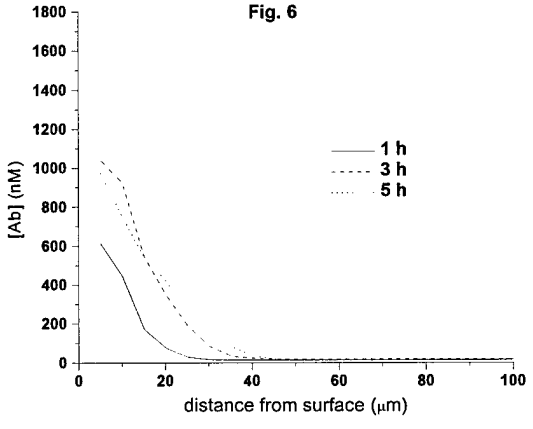

labeled antibody in the field of view. The background signal intensity was used to relate fluorescent intensity to antibody concentration. Using software developed, in house (*3*), and spheroids composed of cells that had been transfected with green fluorescence protein to correct for signal attenuation through the spheroid (*4*), these images were converted to antibody concentration profiles. The results are depicted in figures 5 and 6 for BT474 and MDA MB-361 spheroids, respectively; each curve corresponds to the median of 5 individual spheroid measurements. Details regarding this methodology are provided in reference (*4*). The antibody concentrations profiles show a relatively slow penetration of the antibody with antibody penetration being slightly deeper in the BT474 spheroids than in the MDA MB-361 spheroids. Since the range of alpha particles is typically 80 to 100 μm, complete penetration of antibody is not required to deliver radiation to the spheroid core. The 10 μg/ml antibody concentration used in these studies was, therefore, deemed adequate for the spheroid killing experiments.

Task 3 (month 7-20) - Perform cell kill experiments using Herceptin labeled with Bi-213. Investigate different Bi-213 activity concentrations and specific activities, relevant and irrelevant antibody. Determine optimal Herceptin concentration and Bi-213 activity for each cell line.

Unlabeled Herceptin dose-response

The first step in evaluating the efficacy of alpha-emitter labeled antibody was to determine the efficacy of unlabeled Herceptin for each cell line. In monolayer culture, Herceptin incubation is reported to result in increased cell doubling time leading to increased cell dormancy (*5*). Figures 7 through 9 depict dose-response relationships for BT474, MDA MB-361 and MCF7 spheroids, respectively. Median curves obtained from 24 spheroids per herceptin concentration are shown. One hour incubation with Herceptin antibody concentrations ranging from 10 to 500 μg/ml, did not affect the growth kinetics

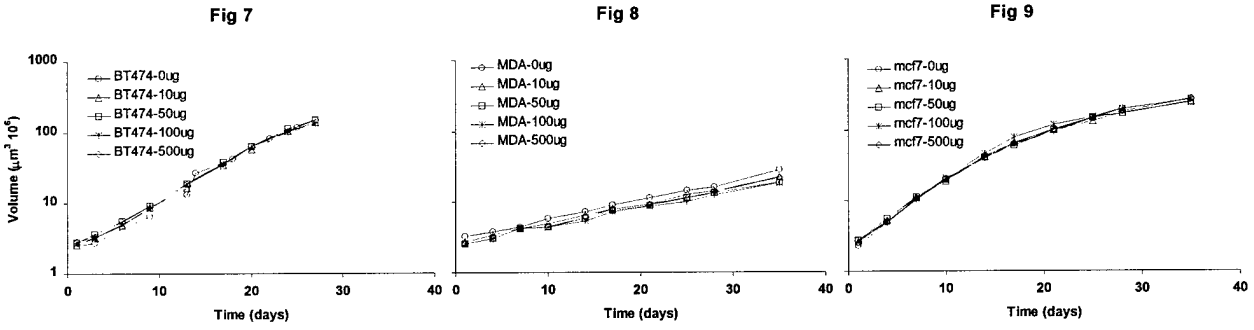

of the spheroids. A one-hour incubation duration was chosen because this was used in the labeled Herceptin spheroid kill experiments. The absence of an effect on spheroids as opposed to monolayer culture is probably the result of incomplete penetration of the Herceptin antibody into spheroids (see above). The known increased resistance to cytotoxic and growth inhibitory agents of spheroids relative to cells in monolayer culture may also play a role (*6*).

Monolayer culture and spheroid radiosensitivities

To discriminate between inherent radiosensitivity of the different cell lines versus differential expression of HER-2/neu, the radiosensitivity of each cell line was determined in monolayer culture using the colony formation assay (*7*). One thousand to ten million cells (depending on radiation dose to be delivered) were plated in monolayer culture and were irradiated using a Cesium irradiator with 3, 6, 9, or 12 Gy. Fractional cell survival curves (surviving fraction, SF vs absorbed dose) are shown in figure 10 for each cell line. Table 1 lists the D_0 values (the amount of absorbed dose required to yield a 37% cell survival fraction).

Fig 10

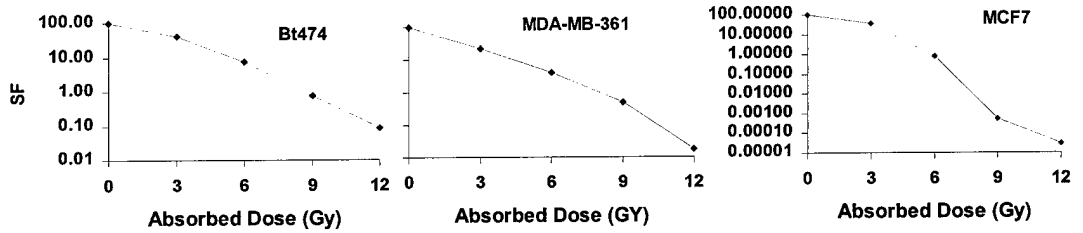

D_0, values were obtained by fitting a monoexponential function, $SF = \exp(-D/D_0)$, to the data shown in figure 10. The results show that the two HER-2/neu receptor positive cell lines are approximately equivalent in radiosensitivity, whereas MCF-7, the low HER-2/neu expressing line is approximately 2-fold more radiosensitive. It is important to note that although these results provide some indication of likely spheroid radiosensitivity against alpha-particles, the numbers can not be translated directly to spheroid kill experiments because alpha particles have a greater biological efficacy per unit absorbed dose (*7*) and because cells derived from spheroids have exhibited a reduced radiosensitivity relative to cells in monolayer culture (*6*). These experiments will be repeated using alpha particles and spheroids. Preliminary results with BT474 spheroids for external (photon) irradiation are shown in figure 11. The median volume of 12 individual spheroids per absorbed dose are plotted. Cell viability in spheroids that had stopped growing was assessed using the spheroid control assay (*8*), in which remaining spheroids are placed in monolayer culture and the fraction of plated spheroids that gives rise to colonies is counted after 20 to 30 days. At the 9 and 12 Gy dose levels, 11/12 and 0/12, respectively, formed colonies.

Table 1- radiosensitivity	
Cell line	D_0 (Gy)
BT474	0.32
MDA MB-361	0.28
MCF7	0.14

Fig. 11

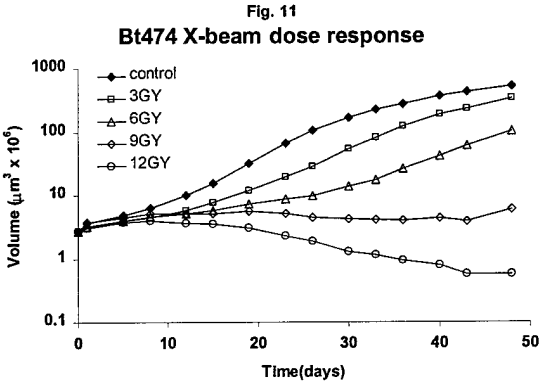

Spheriod kill with radiolabeled Herceptin

The alpha-particle emitting radionuclide, Bi-213, has been replaced with Ac-225, also an alpha-particle emitter. This was necessary because of limited Bi-213 availability. Ac-225 has a 10-day half-life as compared to 45.6 min. for Bi-213. This makes the labeling and handling of this radionuclide easier, both for experimental work and for eventual clinical implementation. Complete decay of Ac-225 and its daughters yields 4 alpha particles compared to one alpha-particle for Bi-213. Ac-225 labeled Herceptin antibody was obtained from the lab. of David Scheinberg, a collaborator on the grant. The purity was generally > 90% and the immunoreactivity of the labeled product was between 70 to 80%. Spheroid kill experiments were carried out by incubating 12 to 24 spheroids with Ac-225-labeled Herceptin or non-specific (hot control) antibody in a 2 ml volume; untreated (control) and unlabeled Herceptin antibody (cold control) were also included as controls. Figures 12 through 14 depict results for BT-474, MDA MB-361 and MCF7 spheroids, respectively. The volume, in $\mu m^3 \times 10^6$ is plotted against time in days; each curve corresponds to the growth history of a single spheroid. All incubations were carried out for 1 hr. Specific and hot control incubations were with 100 nCi/ml Ac-225 on 10 μg/ml antibody. Unlabeled Herceptin at 10 μg/ml was used for the cold control experiments. Radiolabeled anti-leukemia antibody, HuM195, was used for the hot control experiments. These preliminary results show a strong cytotoxic effect of Ac-225-labeled Herceptin at a radioactivity concentration of 100 nCi/ml for BT474 (high HER-2/neu expressing) spheroids. The lower right quadrant of figure 12 shows that 24/24 spheroids disaggregated 50 to 60 days after treatment. As shown on the lower left quadrant,

Fig. 12

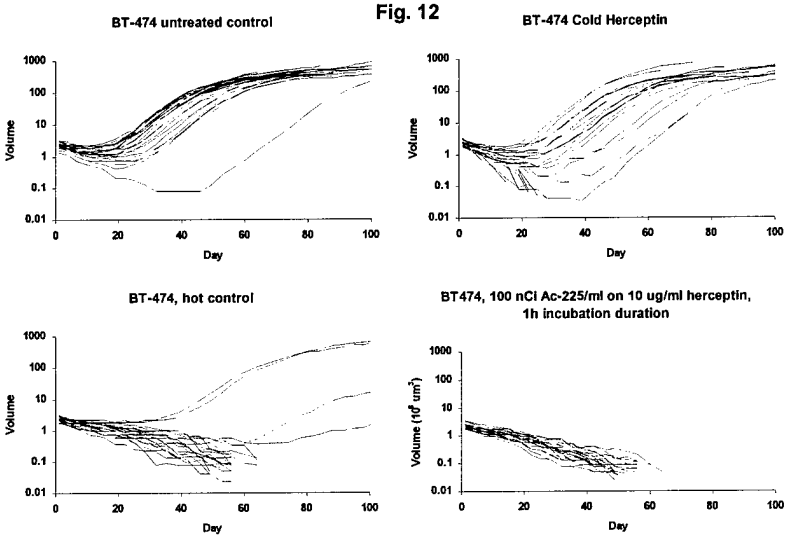

Fig. 13

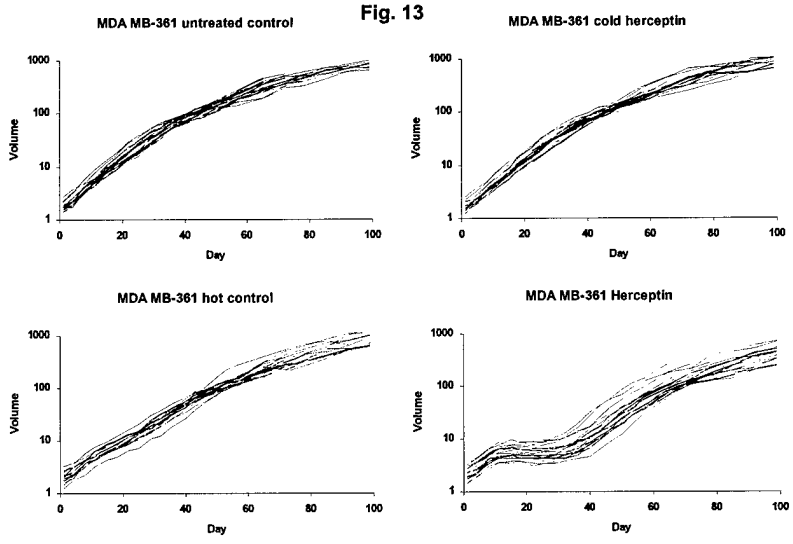

however, this activity concentration leads to overkill since the non-specific antibody also yielded substantial spheroid kill. In contrast, MDA MB-361 spheroids exhibited only a 20-day growth delay following exposure to Ac-225-labeled Herceptin. The lack of response to non-specific radiolabeled antibody (hot control) suggests that, in contrast to results seen with external beam photon irradiation, MDA MB-361 spheroids may be less sensitive to alpha irradiation than BT474 spheroids. A detailed assessment of alpha radiosensitivity using non-specific antibody is pending (see above). Corresponding results for MCF7 spheroids showed a very slight effect of Ac-225-Herceptin (Fig. 14). Growth monitoring of MCF7 spheroids was stopped at approximately 60 days because the spheroids had become too large for further monitoring by optical microscopy. Figures 12 through 14 provide preliminary evidence suggesting that the efficacy of radiolabeled herceptin depends upon the antigen expression. The high spheroid kill rate for hot control in the BT474 experiments suggests a differential radiosensitivity of the spheroids to alphas that is not predicted by the external photon radiosensitivity measurements. These preliminary results for MDA MB-361 have been confirmed and extended in the dose-response results shown on figure 15. In this set of experiments, the radioactivity concentration of Ac-225 was varied while keeping the Herceptin concentration fixed at 10 μg/ml; all other conditions are identical to those for the experiments shown above.

Fig. 14

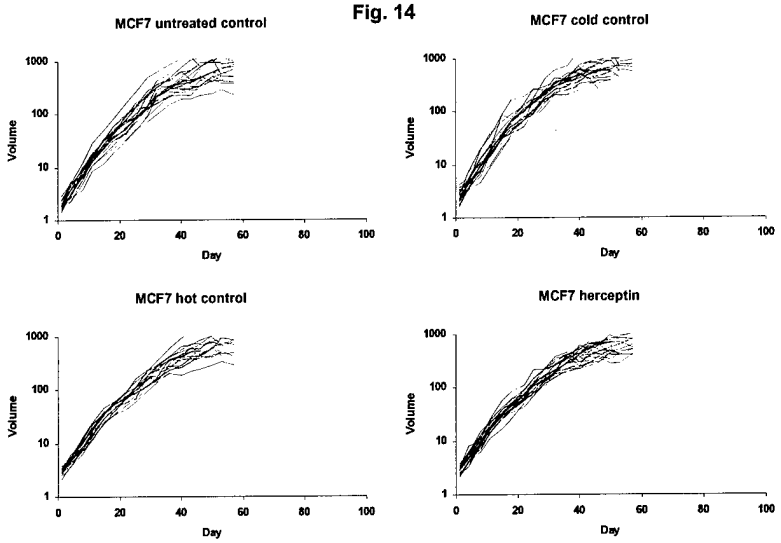

Fig. 15

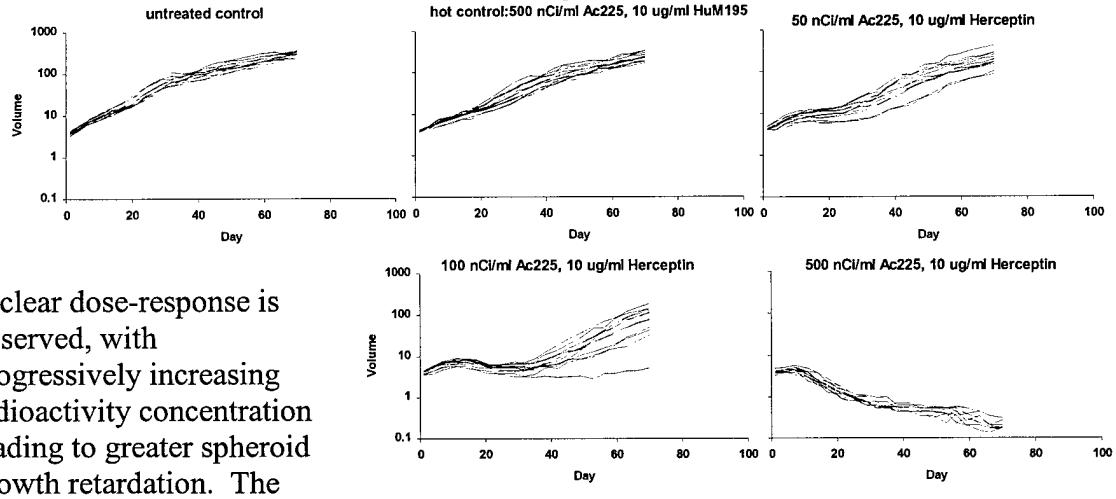

A clear dose-response is observed, with progressively increasing radioactivity concentration leading to greater spheroid growth retardation. The

hot control caused minimal spheroid growth retardation at an activity concentration that yields complete spheroid kill for the specific antibody. The hot control results appear to confirm the high radioresistance of these spheroids. The results also suggest that the optimal activity concentration may lie between 100 and 500 nCi/ml. At 500 nCi/ml, 0/12 spheroids yielded colonies upon plating in monolayer culture. All spheroids exhibitied growth at 100 nCi/ml. Typical optical microscopy images of MDA MB-361 spheroids at different times (in days) after treatment are shown in figures 16 through 20. Similar dose-response studies will be conducted for the other 2 spheroid systems, the impact of different antibody concentrations will also be examined in the remainder time that is left for completion of task 3.

Fig. 16 - MDA MB-361 Untreated

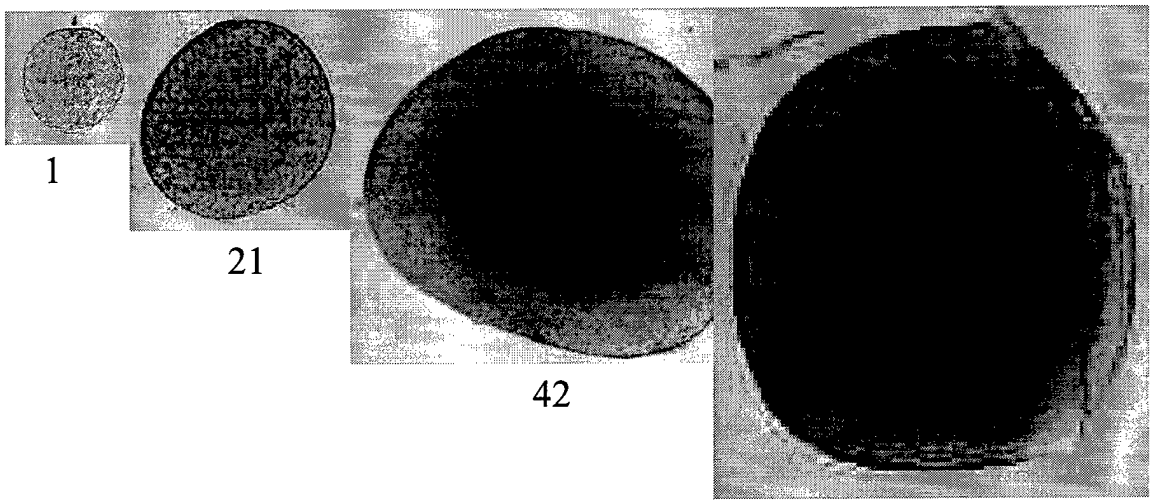

Fig. 17 - MDA MB-361 hot control
(500 nCi/ml Ac-225 on 10 ug/ml HuM195 Ab)

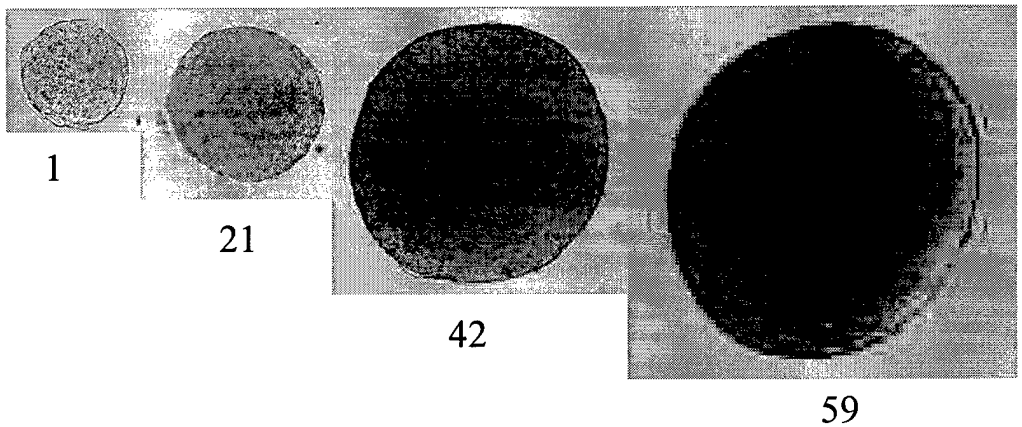

Fig. 18 - MDA MB-361 specific, level 1
(50 nCi/ml Ac-225 on 10 ug/ml Herceptin)

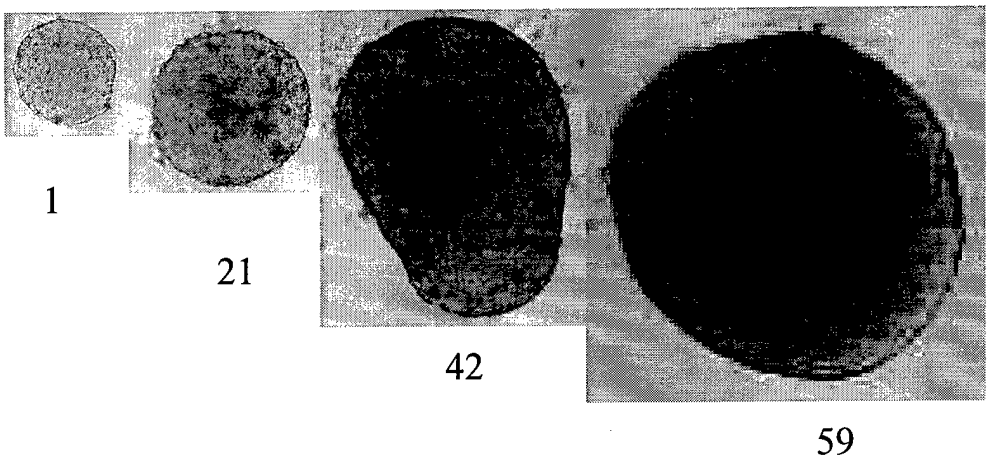

Fig. 19 - MDA MB-361 specific, level 2
(100 nCi/ml Ac-225 on 10 ug/ml Herceptin)

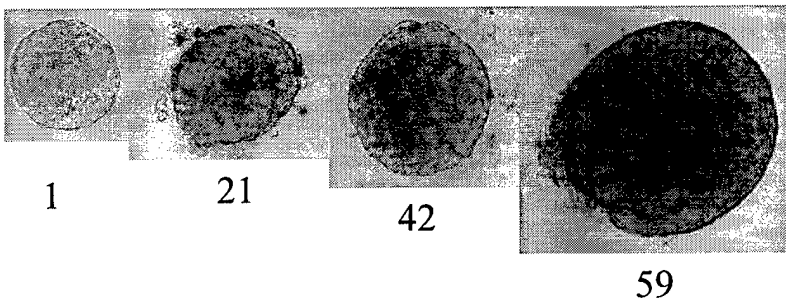

Fig. 20 - MDA MB-361 specific, level 3
(500 nCi/ml Ac-225 on 10 ug/ml Herceptin)

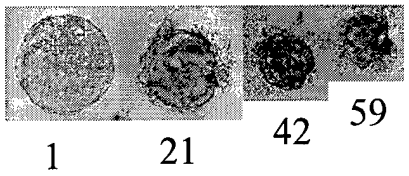

KEY RESEARCH ACCOMPLISHMENTS

- Generated and characterized the growth of spheroids expressing different levels of HER-2/neu receptor.
- Evaluated the radiosensitivities of the three cell lines used for generating the spheroids.
- Characterized antibody penetration kinetics into HER-2/neu expressing spheroids.
- Evaluated the response of HER-2/neu expressing spheroids to Herceptin and to Ac-225 labeled antibody
- Preliminary demonstration of the feasibility of controlling tumor cell clusters with intermediate expression of HER-2/neu.

REPORTABLE OUTCOMES

none

CONCLUSIONS

Work carried out this first year of the funding period concentrated primarily on model development and characterization. During this period spheroids derived from cells with high, intermediate, and low levels of HER-2/neu expression were generated and characterized. These models are critical to the successful completion of the work and to the development of a strategy for targeting breast cancer metastases that may not express HER-2/neu at the high levels required for unlabeled Herceptin treatment.

Dose-response results obtained with MDA MB361 spheroids suggest that it will be possible to eradicate tumor cells with intermediate expression of HER-2/neu using Ac-225-labeled herceptin at a concentration between 100 and 500 nCi/ml. Scaled up to human administration, assuming an initial distribution volume of 3L (i.e., the plasma volume), this activity concentration translates to approximately a 1 mCi injection of ^{225}Ac-Herceptin. Based on animal studies, this activity concentration is clinically realistic (*9*).

SO WHAT? These preliminary studies suggest that by using Herceptin antibody radiolabeled with an alpha-particle emitter it may be possible to treat breast cancer patients whose tumor does not demonstrate high expression of HER-2/neu.

REFERNCES

(*1*) Yuhas JM, Li AP, Martinez AO, Ladman AJ: A simplified method for production and growth of multicellular tumor spheroids. Cancer Res 1977;37:3639-43.

(*2*) Ballangrud AM, Yang WH, Dnistrian A, Lampen NM, Sgouros G: Growth and characterization of LNCaP prostate cancer cell spheroids. Clin Cancer Res 1999;5:3171s-76s.

(3) Kolbert KS, Sgouros G: Display and manipulation of SPECT and CT studies for radiolabeled antibody therapy. Cancer Biother Radiopharm 1998;13:302.

(4) Ballangrud AM, Yang WH, Charlton DE, McDevitt MR, Hamacher KA, Panageas KS, et al: Response of LNCaP spheroids after treatment with an alpha-particle emitter (213Bi)-labeled anti-prostate-specific membrane antigen antibody (J591). Cancer Res 2001;61:2008-14.

(5) Sliwkowski MX, Lofgren JA, Lewis GD, Hotaling TE, Fendly BM, Fox JA: Nonclinical studies addressing the mechanism of action of trastuzumab (Herceptin). Semin Oncol 1999;26:60-70.

(6) Olive PL, Durand RE: Drug and radiation resistance in spheroids: cell contact and kinetics. Cancer Metastasis Rev 1994;13:121-38.

(7) Hall EJ: Assays for dose-response relationships. Radiobiology for the Radiologist, 4th Edition. Philadelphia: J. B. Lippincott Co., 1994, p. 46-47.

(8) Stuschke M, Budach V, Kalff RL, Sack H, Bamberg M, Reinhardt V, et al: Spheroid control of malignant glioma cell lines after fractionated irradiation: relation to the surviving fractions at 2 Gy and colony forming efficiencies in a soft agar clonogenic assay. Radiother Oncol 1993;27:245-51.

(9) McDevitt MR, Ma D, Lai L, Borchardt P, Pellegrini VA, Curcio MJ, et al: Targeting alpha particle emitting isotope generators to tumors: Treatment of model disseminated lymphoma and prostate cancer. J Nucl Med 2001;42:316P.

APPENDIX A – supplementary figures

1. output of FACS analysis showing relative HER-2/neu expression density on BT474, MDA MB-361 and MCF7 cells.

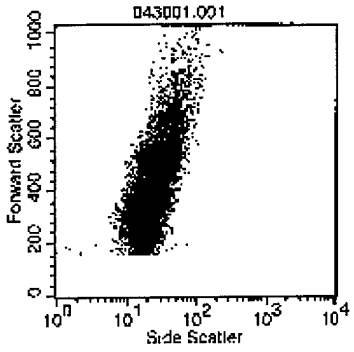

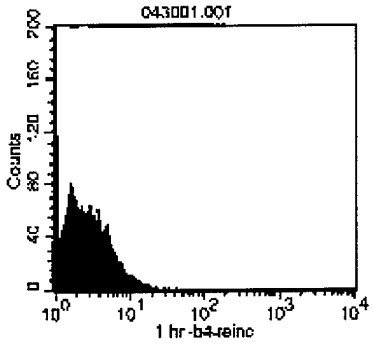

Histogram Statistics

File: 043001.001
Sample ID: MCF7 cells only
Tube:
Acquisition Date: 30-Apr-1
Gated Events: 10000
X Parameter: FL1-H 1 hr b4 reinc (Log)

Log Data Units: Linear Values
Patient ID:
Panel:
Gate: No Gate
Total Events: 10000

Marker	Left, Right	Events	% Gated	% Total	Mean	Geo Mean	CV	Median	Peak Ch
All	1, 9910	10000	100.00	100.00	3.06	2.50	75.84	2.31	1

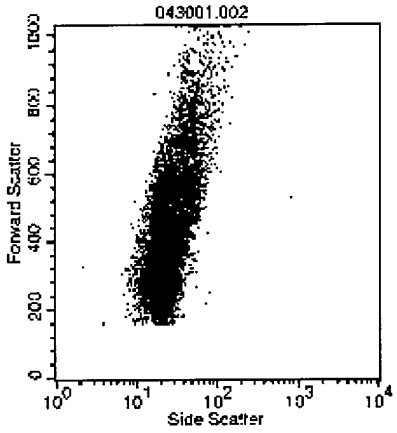

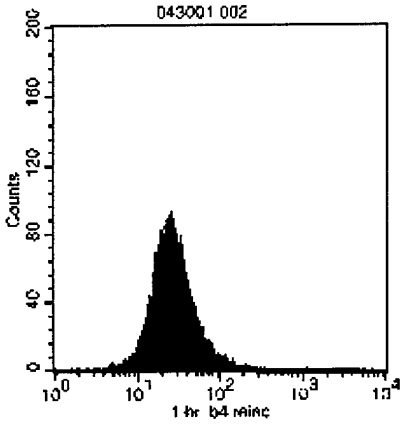

Histogram Statistics

File: 043001.002
Sample ID: MCF7 her2
Tube:
Acquisition Date: 30-Apr-1
Gated Events: 10000
X Parameter: FL1-H 1 hr b4 reinc (Log)

Log Data Units: Linear Values
Patient ID:
Panel:
Gate: No Gate
Total Events: 10000

Marker	Left, Right	Events	% Gated	% Total	Mean	Geo Mean	CV	Median	Peak Ch
All	1, 9910	10000	100.00	100.00	30.97	26.28	77.32	25.48	24

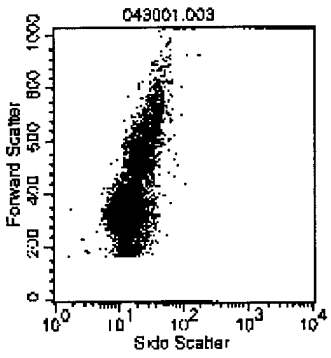

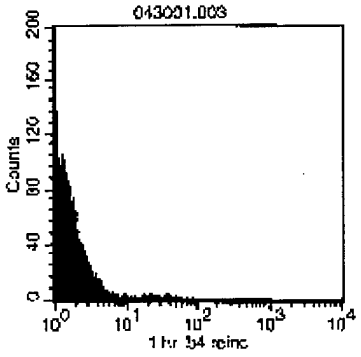

Histogram Statistics

File: 043001.003
Sample ID: MDA cells only
Tube:
Acquisition Date: 30-Apr-1
Gated Events: 10000
X Parameter: FL1-H 1 hr b4 reinc (Log)

Log Data Units: Linear Values
Patient ID:
Panel:
Gate: No Gate
Total Events: 10000

Marker	Left, Right	Events	% Gated	% Total	Mean	Geo Mean	CV	Median	Peak Ch
All	1, 9910	10000	100.00	100.00	1.87	1.52	156.29	1.36	1

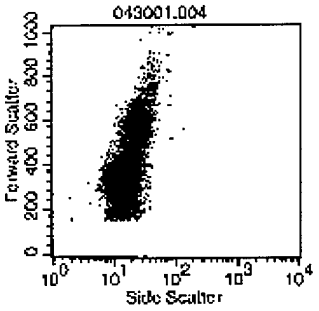

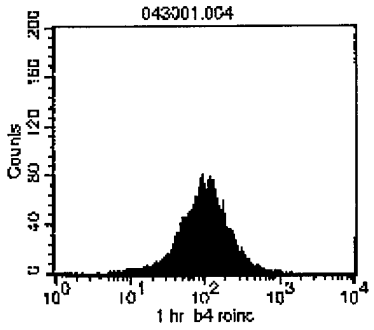

Histogram Statistics

File: 043001.004
Sample ID: MDA her 2
Tube: [illegible]
Acquisition Date: 30-Apr-1
Gated Events: 10000
X Parameter: FL1-H 1 hr b4 reinc (Log)

Log Data Units: Linear Values
Patient ID:
Panel:
Gate: No Gate
Total Events: 10000

Marker	Left, Right	Events	% Gated	% Total	Mean	Geo Mean	CV	Median	Peak Ch
All	1, 9910	10000	100.00	100.00	118.86	96.09	74.84	98.22	89

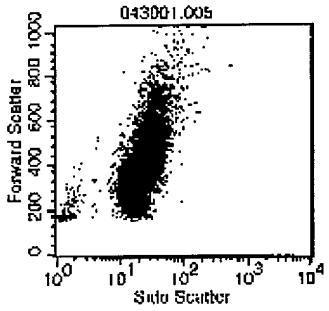

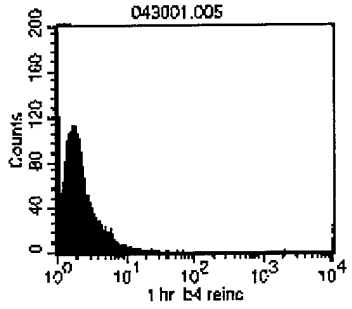

Histogram Statistics

File: 043001 005
Sample ID: BT474 cells only
Tube:
Acquisition Date: 30-Apr-1
Gated Events: 10000
X Parameter: FL1-H 1 hr b4 reinc (Log)

Log Data Units: Linear Values
Patient ID:
Panel
Gate: No Gate
Total Events: 10000

Marker	Left, Right	Events	% Gated	% Total	Mean	Geo Mean	CV	Median	Peak Ch
All	1, 9910	10000	100.00	100.00	2.56	2.02	744.16	1.83	1

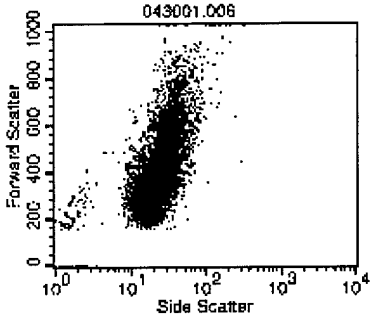

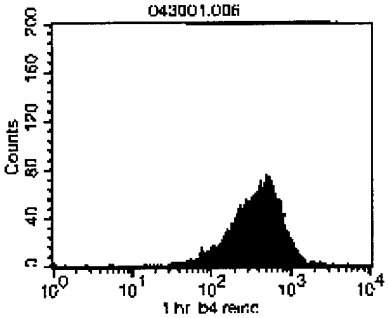

Histogram Statistics

File: 043001 006
Sample ID: BT474 her 2
Tube:
Acquisition Date: 30-Apr-1
Gated Events: 10000
X Parameter: FL1-H 1 hr b4 reinc (Log)

Log Data Units: Linear Values
Patient ID:
Panel:
Gate: No Gate
Total Events: 10000

Marker	Left, Right	Events	% Gated	% Total	Mean	Geo Mean	CV	Median	Peak Ch
All	1, 9910	10000	100.00	100.00	424.72	349.92	61.08	385.42	469

APPENDIX B - manuscripts

1. Ballangrud AM, Yang WH, Dnistrian A, Lampen NM, Sgouros G: Growth and characterization of LNCaP prostate cancer cell spheroids. Clin Cancer Res 1999;5:3171s-76s.
2. Ballangrud AM, Yang WH, Charlton DE, McDevitt MR, Hamacher KA, Panageas KS, et al: Response of LNCaP spheroids after treatment with an alpha-particle emitter (213Bi)-labeled anti-prostate-specific membrane antigen antibody (J591). Cancer Res 2001;61:2008-14.

Growth and Characterization of LNCaP Prostate Cancer Cell Spheroids[1]

Åse M. Ballangrud, Wei-Hong Yang, Ann Dnistrian, Nina M. Lampen, and George Sgouros[2]

Departments of Medical Physics [Å. M. B., W-H. Y., G. S.], Clinical Chemistry [A. D.], and Electron Microscopy [N. M. L.], Memorial Sloan-Kettering Cancer Center, New York, New York 10021

Abstract

Cells from the prostate tumor cell line LNCaP have been grown as spheroids. The growth kinetics of the spheroids have been characterized by fitting a Gompertz equation to spheroid growth curves. The proliferation state of cells within spheroids of different diameters was assessed by bromodeoxyuridine staining. Scanning and electron transmission microscopy were performed to determine the ultrastructure of the spheroids. Prostate-specific antigen (PSA) secretion was monitored throughout spheroid growth. Consistent with Gompertzian kinetics, the volume of LNCaP spheroids initially increased exponentially and then reached a plateau. The doubling time during the exponential phase was 29 ± 4 h. A core of nonproliferating cells was seen in spheroids with a diameter of 400 μm; at a diameter of 600 μm, a necrotic core had formed. In smaller, 200-μm diameter spheroids, a core of nonproliferating cells was not seen, but proliferating cells were concentrated at the spheroid periphery. Electron microscopy showed that the spheroids were enveloped by an extracellular matrix and that cell adhesion within the spheroids was due in part to desmosomes. PSA secretion by the spheroids could be modeled as originating from a spherical shell whose thickness was independent of overall spheroid diameter. The shell thickness obtained by fitting an appropriate equation to the data was consistent with that determined from the bromodeoxyuridine studies. LNCaP cells exhibit several important features of prostate cancer cells; *in vivo*, they are androgen responsive, and they express prostatic acid phosphatase, PSA, and prostate-specific membrane antigen. LNCaP spheroids provide a simple but relevant model for the study of drug delivery and response in prostate cancer.

Introduction

Multicellular tumor spheroids have been used as experimental models in the study of tumor cell metastases (1–8). The spheroid model system offers many of the advantages in terms of experimental manipulation and analysis that are inherent in monolayer tissue cultures, yet it exhibits many of the properties seen in prevascularized tumors growing *in vivo* (9). Spheroids of the prostate cancer cell lines DU-145 and 1-LN have been previously reported and used in the investigation of antibody penetration and treatment response (10–13). In this work, we report on the formation of prostate carcinoma spheroids using the LNCaP cell line (14, 15). Mathematical fitting of spheroid volume and PSA[3] (1) release measurements to the appropriate equations were used to quantitatively characterize the growth and PSA production characteristics of these spheroids. EM was used to examine the ultrastructure of the spheroids and the mechanism of cell-cell attachment. Cell viability and proliferative capacity at different depths within spheroids of different diameters were assessed by BrdUrd staining. LNCaP cells exhibit properties that are highly representative of prostate carcinoma *in vivo*. They exhibit metastatic potential, are androgen responsive, and also produce the three prostatic biomarkers prostatic acid phosphatase, PSA, and prostate-specific membrane antigen (14, 16).

Materials and Methods

Cells

LNCaP (LNCaP-FGC) cells were purchased from the American Type Culture Collection (Manassas, VA). LNCaP-FGC is the cell line that is commonly used in animal studies and is commonly referred to as LNCaP. The FGC designation refers to a fast-growing clone of the original LNCaP cell line (15). Monolayer cultures were incubated in RPMI 1640 (Life Technologies, Inc., Grand Island, NY) supplemented with 10% fetal bovine serum (Gemini Bio-Products, Inc.), 100 units/ml penicillin, and 100 μg/ml streptomycin. The cell cultures were kept at 37°C in a humidified 5% CO_2 and 95% air incubator.

Spheroids

Spheroids were initiated using the liquid overlay technique (17). Cells for spheroid formation were obtained by trypsinization from growing monolayer cultures. Approximately 2×10^6 LNCaP cells were seeded into 100-mm dishes coated with a thin layer of 1% agar (Bacto Agar; Difco, Detroit, MI) with 15 ml of RPMI 1640 supplemented with 10% fetal bovine serum, 100 units/ml penicillin, and 100 μg/ml streptomycin. The plates were incubated at 37°C in a humidified 5% CO_2 and 95% air atmosphere. After an incubation period of 4–6 days, spheroids of 100–150 μm in diameter were selected using an inverted phase microscope and transferred to individual wells coated

[1] Presented at the "Seventh Conference on Radioimmunodetection and Radioimmunotherapy of Cancer," October 15–17, 1998, Princeton, NJ. Supported by NIH National Cancer Institute Grant CA72683.

[2] To whom requests for reprints should be addressed, at Department of Medical Physics, Memorial Sloan-Kettering Cancer Center, 1275 York Avenue, New York, NY 10021. Phone: (212) 639-2127; Fax: (212) 717-3010; E-mail: sgourosg@mskcc.org.

[3] The abbreviations used are: PSA, prostate-specific antigen; BrdUrd, bromodeoxyuridine; EM, electron microscopy.

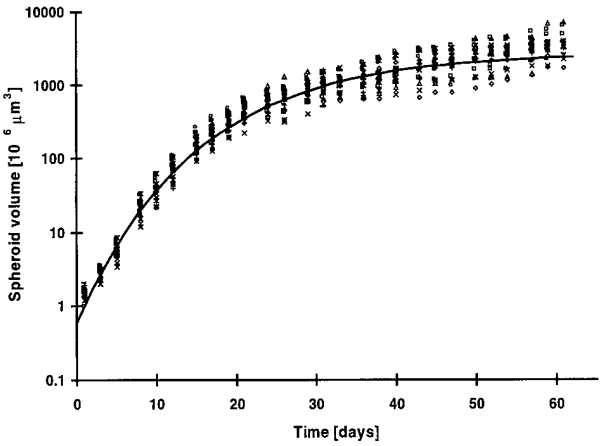

Fig. 1 Fitted growth curve of individual LNCaP spheroids. Each point represents one spheroid. Growth of each spheroid was monitored separately; the data are combined to depict overall growth kinetics. The *solid line* was obtained using the Gompertz equation and the parameters listed in Table 1.

Table 1 The Gompertzian equation was fitted to spheroid growth curves, and the growth kinetic parameters a, b, and V_0 were determined

T and V_{max} were calculated from a, b, and V_0. The parameters are determined individually for each spheroid, and average values ± SD are listed.

Growth parameters	LNCaP cells
V_0 (10^6 µm^3)	0.6 ± 0.2
a (day^{-1})	0.57 ± 0.07
b (day^{-1})	0.068 ± 0.008
T (h)	29 ± 4
V_{max} (10^6 µm^3)	3078 ± 1277

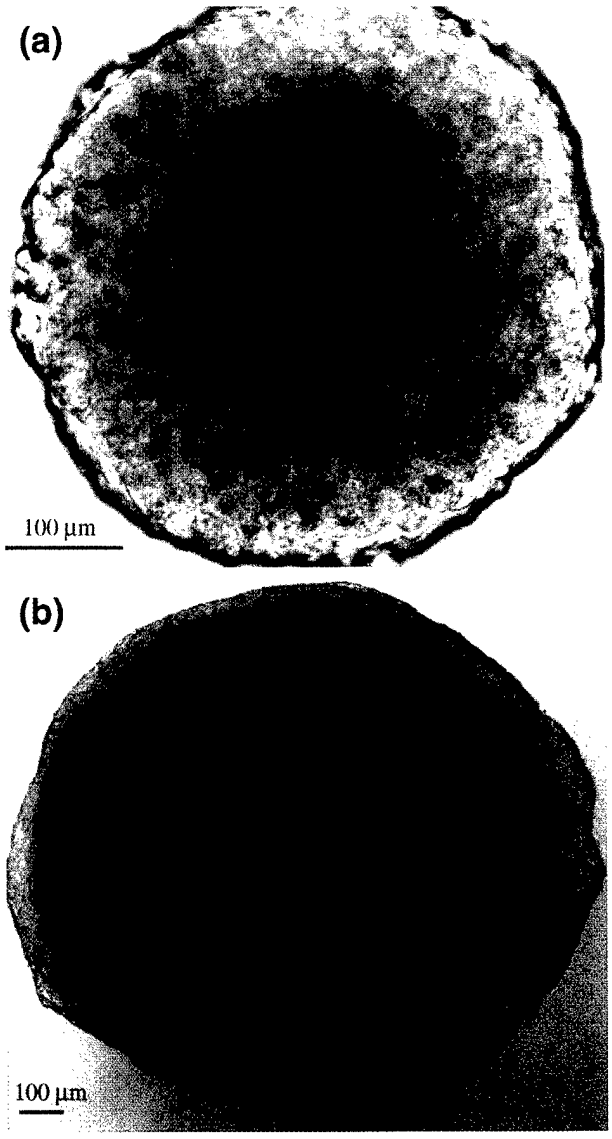

Fig. 2 Light microscope image of a spheroid at (*a*) day 12 and (*b*) day 39.

with a thin layer of 1% agar. The medium was changed three times per week. Light microscopy images were acquired using an inverted phase microscope (Axiophot 2; Carl Zeiss Ltd., Göttingen, Germany) fitted with a digital camera (EOS-DCS 5; Kodak, Rochester, NY).

Characterization of Spheroid Growth

The major (d_{max}) and minor (d_{min}) diameters for each of 24 spheroids growing in a 24-well plate were determined using an inverted phase microscope fitted with an occular micrometer. Spheroid volume was calculated as $V = \pi \times d_{max} \times d_{min}^2/6$. The volume-*versus*-time curves [$V(t)$] of 24 individual spheroids were each fit to the Gompertz equation (18–20):

$$V(t) = V_0 \exp\left(\frac{a}{b}(1 - \exp(-bt))\right) \quad \text{(A)}$$

where V_0 is the initial volume of the spheroid, a is the maximum potential growth rate, b is the rate at which growth slows down, and t is the time elapsed since the initial volume measurement. The simulation analysis and modeling software package (SAAM II, version 1.1; SAAM Institute Inc., Seattle, WA) was used to perform the fits (21, 22). The potential doubling time (T) of tumor cells making up the spheroid can be calculated as $T = \ln(2)/a$, and the asymptotic maximum spheroid volume is given as $V_{max} = V_0\ exp(a/b)$.

BrdUrd Staining

Tumor cell viability within spheroids of different diameters was assessed by BrdUrd staining. After a 62-h incubation with 10 µM BrdUrd, spheroids were washed with cold medium and then placed in OCT-filled cryomolds. A long incubation period was used to increase diffusion into the spheroids. Frozen blocks were produced by immersion into a dry ice-ethanol bath. Serial 5-µm sections of the frozen blocks were made using a cryotome and mounted on poly-L-lysine-coated slides that were fixed in hydrogen peroxide with 90% methanol. BrdUrd staining was performed using a biotinylated mouse antibody against BrdUrd

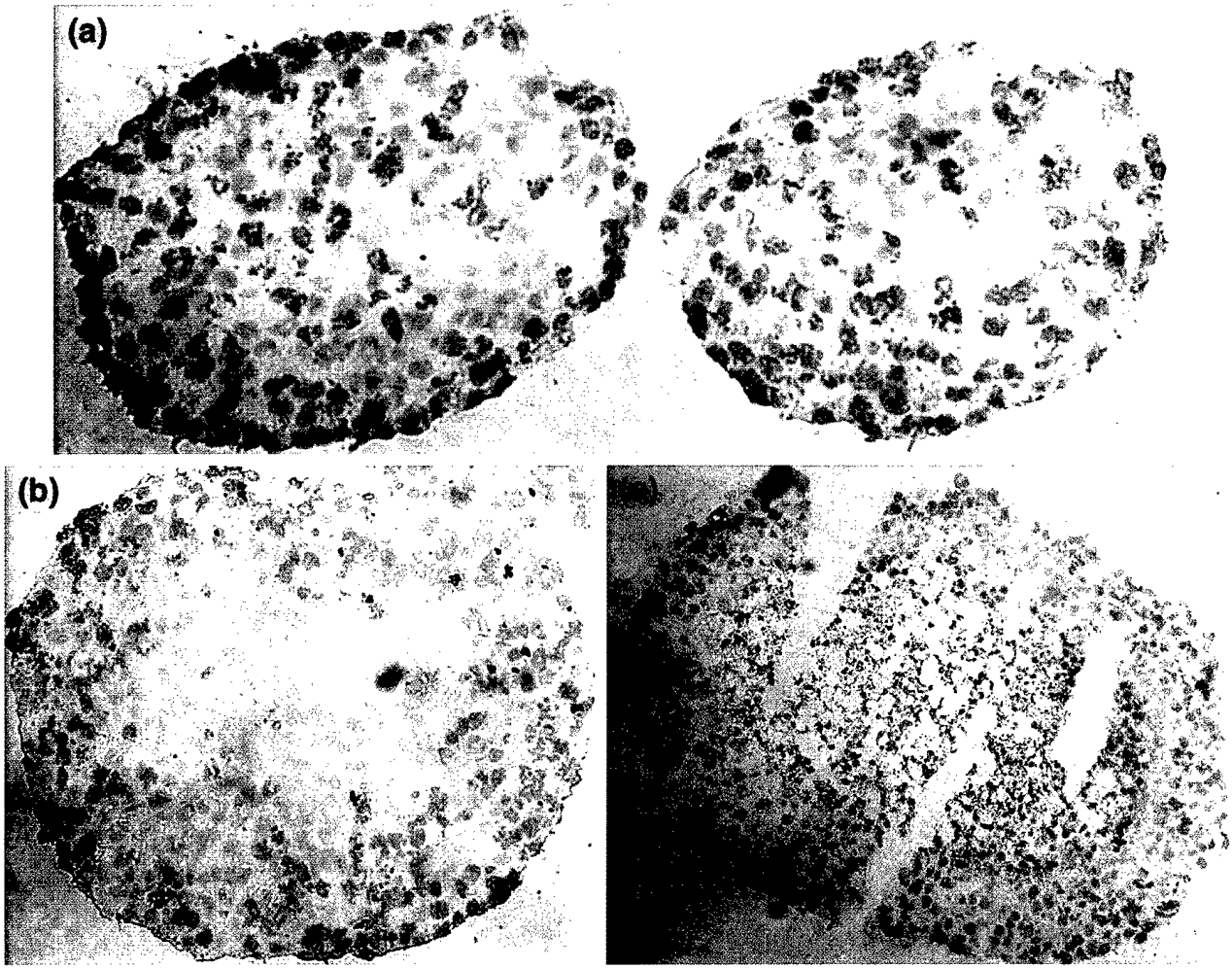

Fig. 3 Light microscope images of 5-μm spheroid sections stained for BrdUrd (*brown*) and counterstained with H&E. Spheroids with diameters of (*a*) 200, (*b*) 400, and (*c*) 600 μm are shown.

and streptavidin-peroxidase (BrdUrd Staining Kit; Calbiochem, Oncogene Research Products, Cambridge MA).

EM

Transmission EM. Spheroid pellets were fixed in 2.5% glutaraldehyde, treated with 2% OsO_4, rinsed with distilled H_2O, dried using alcohol, and embedded in Poly/Bed 812. Thin sections were obtained using a Sorvall Ultra-Microtome MT-2 and photographed using a JEOL 1200-EX electron microscope.

Scanning EM. The spheroids were placed on poly-L-lysine-coated Thermonox plastic coverslips. The 2.5% gluteraldehyde-treated and alcohol-dried samples were then freeze-dried and sputter-coated with gold/palladium in a Technics Hummer V1 sputtering system. The samples were photographed using a JEOL JSM 35 scanning electron microscope.

PSA

PSA was determined by heterogeneous sandwich magnetic separation using an automated clinical immunoassay analyzer (the Technicon Immuno 1 System; Bayer Corp., Tarrytown NY). All PSA determinations were made for spheroids growing in 2 ml of media after 3 days of incubation.

A relationship between spheroid volume and PSA secretion was derived by assuming that PSA is secreted by viable cells only and that it can freely diffuse out of the spheroid. Spheroids that are greater than 300–400 μm in diameter have been characterized as having a hypoxic or necrotic core of cells surrounded by a rim of proliferating cells that remains constant in width over the spheroid diameters examined. In the absence of a necrotic or hypoxic core, all cells within the spheroid would be expected to secrete PSA. Given the assumptions indicated above, PSA secretion as a function of spheroid radius is represented by:

$$A_{PSA} = \begin{cases} f \cdot \frac{4\pi}{3} \cdot r^3 & r < T \\ f \cdot \frac{4\pi}{3} \cdot (r^3 - (r-T)^3) & r \geq T \end{cases} \quad \text{(B)}$$

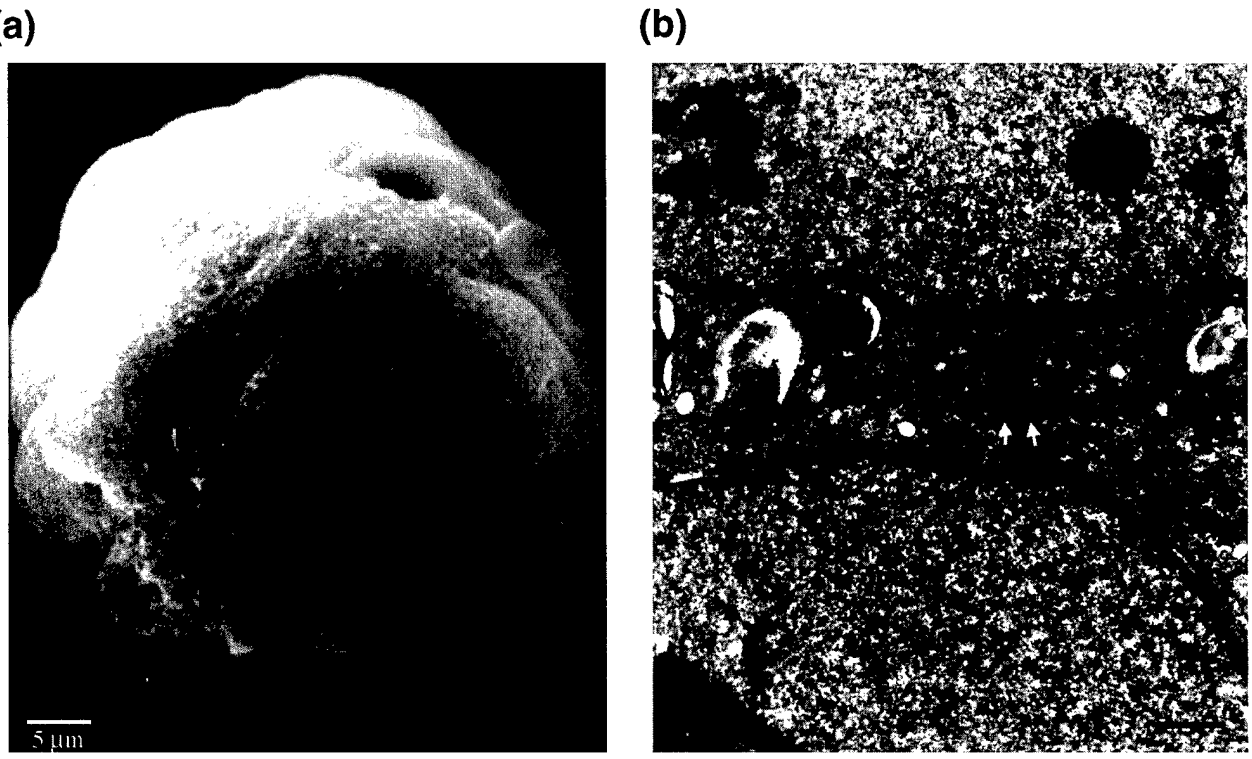

Fig. 4 *a*, scanning EM of 45–50-μm-diameter spheroid. *b*, transmission EM showing a desmosome between the two *white arrows*. *Dark bar* (*bottom right*), 500 nm.

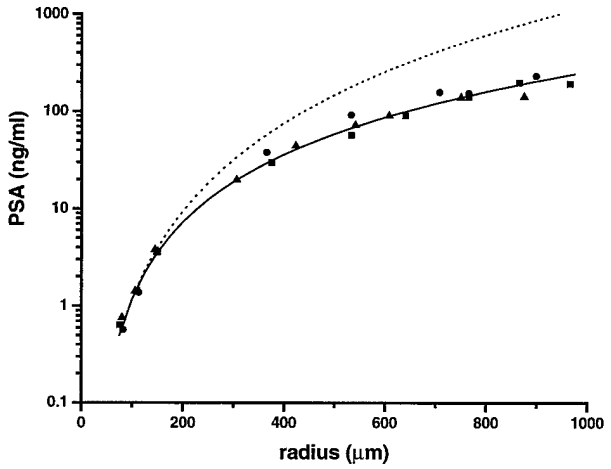

Fig. 5 PSA concentration for three different spheroids, individually identified by a triangle, square or circle. A fit of equation 2 to the data are depicted by the *solid line*. The *dotted line* represents the PSA *versus* spheroid radius expected if all cells in the spheroid were producing PSA.

where r is the radius of the spheroid, T is the thickness of a shell of viable cells, and f is a conversion factor that relates PSA secretion to a volume of viable cells. Parameter f can be obtained from spheroids that do not have a hypoxic or necrotic core, *i.e.*, $r \leq T$. The thickness of viable cells (T) was obtained by fitting measurements of spheroid volume *versus* PSA to Eq. B. The simulation analysis and modeling software package described above (SAAM II, version 1.1) was used to perform the fits.

Results

Fig. 1 depicts growth data for 24 individual LNCaP spheroids followed over a 60-day period. The growth kinetic parameters listed in Table 1 were used with Eq. A to obtain the solid curve shown in the figure. Fig. 2, *a* and *b*, depicts light microscopy images of a typical spheroid 12 and 39 days after the initiation of spheroid growth. On day 12, the spheroid volume is 70×10^6 μm^3 (diameter = 500 μm), corresponding to the rapid growth phase; the spheroid volume on day 39 is 1800×10^6 μm^3 (diameter = 1500 μm), corresponding to the plateau growth phase seen in Fig. 1. Spheroids that are greater than 200 μm in diameter are likely to have a core of cells that do not proliferate. This is shown in the BrdUrd images of Fig. 3. Such a core of nonproliferating tumor cells is clearly evident in a 400-μm-diameter spheroid (Fig. 3*b*). As the spheroid size increases, this core of cells becomes necrotic. This is shown in Fig. 3*c*, which depicts a spheroid with a diameter of 600 μm. At a diameter of 200 μm, there is no such well-delineated core, but the proliferating cells are concentrated toward the periphery of the spheroid (Fig. 3*a*). These observations are consistent with those seen in spheroid models of other cell lines and result from reduced nutrient and oxygen availability at the spheroid core as the spheroid diameter increases (23). Based on the images in Fig. 3, *b* and *c*, and also on other BrdUrd images (data not

shown), the rim of proliferating cells is 76 ± 13 μm thick. Even within this rim of proliferating cells, only approximately 50% of the cells stained with BrdUrd. This suggests that there is a high fraction of nonproliferating or quiescent cells in these spheroids. Similar results have been obtained in other spheroid models (23, 24).

Scanning and transmission EM images of two different spheroids are shown in Fig. 4, *a* and *b*, respectively. Cells making up the 45–50-μm-diameter spheroid in Fig. 4*a* appear to be covered by an extracellular matrix. The connection between cells making up the spheroids may be identified from Fig. 4*b*. The border between the two cell portions appears as a continuous transverse line that spans the middle of the image. Cell-cell attachment via a desmosome is indicated by the dark patch of filaments spanning the two cell membranes (shown between the two *white arrows*). A mitochondrion may be seen immediately above the desmosome, and just above this, the nuclear envelope of the top cell is visible. Cell adhesion by desmosomes provides strong bonds between cells, but only at specific points of contact. This yields a spheroid architecture that would allow the diffusion of larger molecules such as antibodies but is also tightly held together.

The increase in PSA concentration with spheroid radius is shown in Fig. 5 for three different and separately monitored spheroids. The data show an exponential rise in PSA for spheroids below 200 μm in radius; as the spheroids grow, the exponential rate associated with PSA release decreases. A fit of Eq. B to these data yields the solid line shown on the figure. The fitted values for f and T were $2.8 \times 10^{-7} \pm 0.2 \times 10^{-7}$ ng/ml/μm^3 and 77 ± 3 μm, respectively. The figure also shows the PSA concentration curve that would have been obtained if PSA were generated from all cells making up the spheroids (*i.e.*, if PSA production were not limited to a rim of proliferating cells). The value for T obtained from the fit is in good agreement with the average thickness of 76 ± 13 μm obtained from the BrdUrd images.

Discussion

We have grown and characterized spheroids of LNCaP, a prostate carcinoma cell line. Spheroid growth could be described by a Gompertz equation. Spheroids of other human tumor cell lines (10, 25) have also shown Gompertzian growth characteristics. The potential doubling times for spheroids of the breast carcinoma cell line MCF-7 and of the prostate carcinoma cell line DU145 are 46.2 and 120 h, respectively, *versus* 29 h for the LNCaP spheroids obtained in this study. BrdUrd staining to assess cell proliferation showed that a nonproliferating core of cells may be seen at a spheroid diameter of 400 μm, but not at a spheroid diameter of 200 μm. Larger spheroids developed necrotic cores. The 76 μm thickness of the rim of proliferating cells seen in these spheroids is consistent with the 100 μm thickness observed in 800-μm-diameter DU145 spheroids (10). These results suggest that the efficacy of anticancer agents on tumor cells that are proliferating or are viable but nonproliferating may be studied with spheroids by selecting the appropriate initial spheroid diameter. Efficacy studies using spheroids with diameters that are of the order of 1 mm are likely to be heavily influenced by the large core of necrotic cells. Ultrastructure studies of the LNCaP spheroids showed that, as might be expected *in vivo*, desmosomes are partially involved in cell-cell adhesion. PSA production by the spheroids was well predicted as originating from a shell of viable cells. The shell thickness, as predicted by fitting an equation to the data, was consistent with that determined from BrdUrd immunohistochemistry.

The LNCaP cell line is widely used as a model of prostate cancer *in vivo*. Spheroids of this tumor cell line have not been previously reported. Spheroids with initial diameters of 150–200 μm will be used in future studies to model systemic treatment of micrometastases (26). The baseline measurements reported herein will be used to evaluate treatment response. In addition to spheroid growth delay, the results demonstrate that PSA production would be a valuable measure of treatment response. Therefore, this spheroid model provides two of the primary measures for assessing treatment response *in vivo*, but with the advantage that the growth and treatment conditions may be tightly controlled.

Acknowledgments

Digital imaging and microscopy were performed at the Molecular Cytology Core Facility with the assistance of Dr. Katia Manova.

References

1. Sutherland, R. M. Cell and environment interaction in tumor microregions: the multicell spheroid model. Science (Washington DC), *240:* 177–184, 1988.

2. Kwok, C. S., Crivici, A., MacGregor, W. D., and Unger, M. W. Optimization of radioimmunotherapy using human malignant melanoma multicell spheroids as a model. Cancer Res., *49:* 3276–3281, 1989.

3. Langmuir, V. K., McGann, J. K., Buchegger, F., and Sutherland, R. M. ^{131}I-Anticarcinoembryonic antigen therapy of LS 174T human colon adenocarcinoma spheroids. Cancer Res., *49:* 3401–3406, 1989.

4. Bardies, M., Thedrez, P., Gestin, J. F., Marcille, B. M., Guerreau, D., Faivre-Chauvet, A., Mahe, M., Sai-Maurel, C., and Chatal, J. E. Use of multicell spheroids of ovarian carcinoma as intraperitoneal radioimmunotherapy model: uptake, retention kinetics and dosimetric evaluation. Int. J. Cancer, *50:* 984–991, 1992.

5. Lelievre, S., and Larsen, A. K. Development and characterization of suramin-resistant Chinese hamster fibrosarcoma cells: drug-dependent formation of multicellular spheroids and a greatly enhanced metastatic potential. Cancer Res., *54:* 3993–3997, 1994.

6. Walker, K. A., Murray, T., Hilditch, T. E., Wheldon, T. E., Gregor, A., and Hann, I. M. A tumor spheroid model for antibody-targeted therapy of micrometastases. Br. J. Cancer, *58:* 13–16, 1988.

7. Kohno, N., Ohnuma, T., Holland, J. F., and Biller, H. Effects of anticancer agents on the shedding of cells from human multicellular tumor spheroids. Invasion Metastasis, *7:* 264–274, 1987.

8. Bjerkvig, R. (ed.). Spheroid Culture in Cancer Research. Boca Raton, FL: CRC Press, 1992.

9. Davies, C. D., Muller, H., Hagen, I., Garseth, M., and Hjelstuen, M. H. Comparison of extracellular matrix in human osteosarcomas and melanomas growing as xenografts, multicellular spheroids, and monolayer cultures. Anticancer Res., *17:* 4317–4326, 1997.

10. Essand, M., Nilsson, S., and Carlsson, J. Growth of prostate cells, DU 145, as multicellular spheroids and effects of estramustine. Anticancer Res., *13:* 1261–1268, 1993.

11. Sauer, H., Ritgen, J., Hescheler, J., and Wartenberg, M. Hypotonic Ca^{2+} signaling and volume regulation in proliferating and quiescent cells from multicelluar spheroids. J. Cell. Physiol., *175:* 129–140, 1998.

12. Wartenberg, M., Frey, C., Diedershagen, H., Ritgen, J., Hescheler, J., and Sauer, H. Development of an intrinsic P-glycoprotein-mediated doxorubicin resistance in quiescent cell layers of large, multicellular prostate tumor spheroids. Int. J. Cancer, *75:* 855–863, 1998.

13. Donaldson, J. T., Tucker, J. A., Keane, T. E., Walther, P. J., and Webb, K. S. Characterization of a new model of human prostatic cancer: the multicellular tumor spheroid. Int. J. Cancer, *46:* 238–244, 1990.

14. Horoszewicz, J. S., Leong, S. S., Kawinski, E., Karr, J. P., Rosenthal, H., Ming Chu, T., Mirand, E. A., and Murphy, G. P. LNCaP model of human prostatic carcinoma. Cancer Res., *43:* 1809–1818, 1983.

15. Van Steenbrugge, G. J., Groen, M., van Dongen, J. W., Bolt, J., van der Korput, H., Trapman, J., Hasenson, M., and Horoszewicz, J. The human prostatic carcinoma cell line LNCaP and its derivatives. Urol. Res., *17:* 71–77, 1989.

16. Israeli, R. S., Powell, C. T., Corr, J. G., Fair, W. R., and Heston, W. D. W. Expression of the prostate-specific membrane antigen. Cancer Res., *54:* 1807–1811, 1994.

17. Yuhas, J. M., Li, A. P., Martinez, A. O., and Landman, A. J. A simplified method for production and growth of multicellular tumor spheroids. Cancer Res., *37:* 3639–3643, 1977.

18. Gompertz, B. On the nature of the function expressive of the law of human mortality and on a new model of determining life contingencies. Philos. Trans. R. Soc. Lond-Biol. Sci., *115:* 513–585, 1825.

19. Norton, L. A Gompertzian model of human breast cancer growth. Cancer Res., *48:* 7067–7071, 1988.

20. Steel, G. G. Growth Kinetics of Tumors. Oxford, United Kingdom: Clarendon Press, 1977.

21. SAAM Institute. SAAM II User Guide. Seattle, WA: University of Washington, 1997.

22. Foster, D. M., Boston, R. C., Jacquez, J. A., and Zech, L. A. (eds.). The SAAM Tutorials: An Introduction to Using Conversational SAAM Version 30. Resource Facility for Kinetic Analysis. Seattle, WA: University of Washington, 1989.

23. Durand, R. E. Cell cycle kinetics in an *in vitro* tumor model. Cell Tissue Kinet., *9:* 403–412, 1976.

24. Olea, N., Villalobos, M., Ruiz de Almodóvar, J. M., and Pedraza, V. MCF-7 breast cancer cells grown as multicellular spheroids *in vitro*: effect of 17β-estradiol. Int. J. Cancer, *50:* 112–117, 1992.

25. Olea, N., Villalobos, M., Nuñez, M. I., Elvira, J., Ruiz de Almodóvar, J. M., and Pedraza, V. Evaluation of the growth rate of MCF-7 breast cancer multicellular spheroids using three mathematical models. Cell Prolif., *27:* 213–223, 1994.

26. Yang, W-H., Ballangrud, Å. M., McDevitt, M. R., Finn, R. A., Geerlings, M., Bander, N., Scheinberg, D. A., and Sgouros, G. α Particle emitter therapy of micrometastases: 213Bi-J591 (anti-PSMA) treatment of LNCaP spheroids. Proc. Am. Assoc. Cancer Res., *39:* 440, 1998.

[CANCER RESEARCH 61, 2008–2014, March 1, 2001]

Response of LNCaP Spheroids after Treatment with an α-Particle Emitter (^{213}Bi)-labeled Anti-Prostate-specific Membrane Antigen Antibody (J591)[1]

Åse M. Ballangrud, Wei-Hong Yang, David E. Charlton, Michael R. McDevitt, Klaus A. Hamacher, Katherine S. Panageas, Dangshe Ma, Neil H. Bander,[2] David A. Scheinberg, and George Sgouros[3]

Departments of Medical Physics [Å. M. B., W-H. Y., K. A. H., G. S.], Medicine [M. R. M., D. M., D. A. S.], and Epidemiology and Biostatistics [K. S. P.], Memorial Sloan-Kettering Cancer Center, New York, New York 10021; Weill Medical College of Cornell University, New York, New York 10021 [N. H. B.]; and Physics Department, Concordia University, Montreal, Quebec, Canada [D. E. C.]

ABSTRACT

A theoretical drawback to α-particle therapy with ^{213}Bi is the short range of the particle track coupled with the short half-life of the radionuclide, thereby potentially limiting effective cytotoxicity to rapidly accessible, disseminated individual tumor cells (*e.g.*, as in leukemia). In this work, a prostate carcinoma spheroid model was used to evaluate the feasibility of targeting micrometastatic clusters of tumor cells using ^{213}Bi-labeled anti-prostate-specific membrane antigen (PSMA) antibody, J591. In prostate cancer, vascular dissemination of tumor cells or tumor cell clusters to the marrow constitutes an important step in the progression of this disease to widespread skeletal involvement, an incurable state. Such prevascularized clusters are ideal targets for radiolabeled antibodies because the barriers to antibody penetration that are associated with the capillary basal lamina have not yet formed. β- and γ-emitting radionuclides such as ^{131}I, which are widely used in radioimmunotherapy, are not expected to be effective when targeting single cells or small cell clusters. This is because the range of the emissions is one to two orders of magnitude greater than the target size, and the energy deposited per traversal is insufficient to produce any significant radiobiological effect. Spheroids of the prostate cancer cell line, LNCaP-LN3, were used as a model of prevascularized micrometastases; their response to an anti-PSMA antibody, J591, radiolabeled with the α-particle emitter ^{213}Bi ($T_{1/2}$, 45.6 min.) has been measured. The time course of spheroid volume reductions was found to be sensitive to the initial spheroid volume. J591 labeled with 0.9 MBq/ml ^{213}Bi resulted in a 3-log reduction in spheroid volume on day 33, relative to control, for spheroids with an initial diameter of 130 μm; 1.8 MBq/ml were required to achieve a similar response for spheroids with an initial diameter of 180 μm. Equivalent spheroid responses were observed after 12 Gy of acute external beam photon irradiation. Monte Carlo-based microdosimetric analyses of the ^{213}Bi decay distribution in individual spheroids of 130-μm diameter yielded an average α-particle dose of 3.7 Gy to the spheroids, resulting in a relative biological effectiveness factor of 3.2 over photon irradiation. The activity concentrations used in the experiments were clinically relevant, and this work supports the possibility of using ^{213}Bi-labeled antibodies not only for disseminated single tumor cells, as found in patients with leukemia, but also for micrometastatic tumor deposits up to 180 μm in diameter (1200 cells).

INTRODUCTION

Radiolabeled antibody therapy has already demonstrated efficacy in the treatment of non-Hodgkin's lymphoma (1–3). Results have been largely disappointing, however, in the targeting of bulky disease. To target bulky disease, i.v. administered antibody must extravasate, diffuse across an interstitial fluid space, and then distribute throughout antigen-positive cells. Each of these steps is associated with a barrier to delivery (4–9). By targeting hematologically distributed, single tumor cells or tumor cell clusters, the barriers to antibody delivery are diminished.

β-Particle-emitting radionuclides such as ^{131}I and ^{90}Y have been used in most applications of radioimmunotherapy. These radionuclides are suboptimal for sterilizing single tumor cells or small tumor cell clusters because the concentration of radioactivity required to provide the thousands to tens of thousands of β-particle traversals through the cell nucleus needed to achieve cytotoxicity would also yield prohibitive normal organ toxicity. α-Particles are much more cytotoxic than β-particles and would, therefore, be ideal candidates in targeting individual tumor cells or small clusters. The effectiveness of α-particles arises because the amount of energy deposited per unit distance traveled (linear energy transfer) can be several orders of magnitude greater than that of β-particles. Cell survival studies have shown that α-particle-induced killing is independent of oxygenation state or cell cycle during irradiation (10, 11).

Spheroids have been used by a number of investigators as models of tumor cell micrometastases (12–17). These multicellular clusters provide the experimental flexibility of monolayer cultures while preserving the three-dimensional structure that is important for the cell-to-cell interaction that exists *in vivo*. The spheroid model is particularly important in establishing a relationship between antibody binding kinetics, antigen density, internalization, and external antibody concentration, as well as to assess kill probability under different antibody concentrations and specific activities. It is an ideal model to optimize treatment parameters. Such optimization is essential in the treatment of micrometastases because objective measures of response will not be generally available *in vivo*.

Previous spheroid studies with large (800-μm-diameter) spheroids using antibodies labeled with the α-particle emitter, ^{212}Bi, concluded that this α-particle emitter would be ineffective because the short, 50–90-μm range of the α-particles, coupled with the short, 1-h half-life, restricted tumor cell targeting (18). The requirement of adequate oxygen and nutrient supply, however, limits prevascularized micrometastases to maximum diameters of 150–200 μm. The emission properties of ^{213}Bi (Fig. 1) used in the experiments reported here are similar to those of ^{212}Bi, with the exception that ^{213}Bi does not emit the highly energetic and penetrating photon emissions found in ^{212}Bi. Recently, Kennel *et al.* (19) compared surviving fraction of cells in monolayers and in spheroids irradiated by surface-bound ^{213}Bi. These studies were carried out using spheroids derived from the murine EMT6 cell line and the 13A antibody against murine CD44. Tumor cells in spheroids were efficiently killed for spheroids up to 20–30 cells in diameter. Animal studies have also been performed and show that α-particle emitters yield superior tumor control relative to β or Auger electron emitters (10, 20–23). Human use of α-particle emitters has also been reported (24–26). The first implementation was with ^{213}Bi conjugated to the anti-CD33 antibody, HuM195, targeting myeloid leukemia. This trial demonstrated feasibility and anticancer activity with minimal toxicity (24). The anti-tenascin antibody, 81C6,

Received 8/8/00; accepted 1/3/01.

The costs of publication of this article were defrayed in part by the payment of page charges. This article must therefore be hereby marked *advertisement* in accordance with 18 U.S.C. Section 1734 solely to indicate this fact.

[1] Supported, in part, by NIH Grants PO1 CA-33049, R01 CA-55349, and R01 CA-72683 and also by the CapCure Foundation. D. A. S. is the recipient of the Doris Duke Distinguished Clinical Scientist Award.

[2] N. H. B. is a consultant to BZL Biologics, Inc. His association with BZL is managed in accordance with the conflict of interest policies of Cornell University.

[3] To whom requests for reprints should be addressed, at Department of Medical Physics, Memorial Sloan-Kettering Cancer Center, 1275 York Avenue, New York, NY 10021. E-mail: sgourosg@mskcc.org.

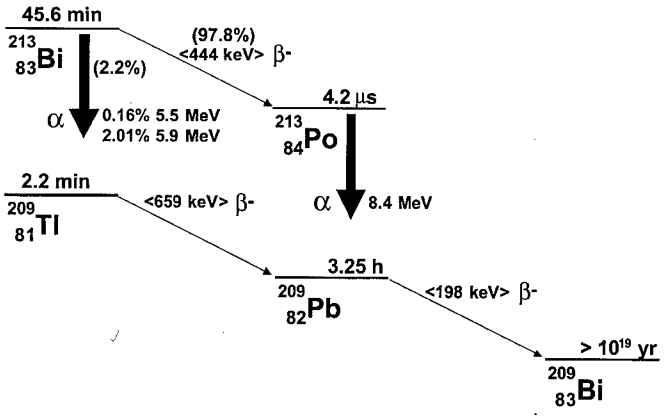

Fig. 1. ^{213}Bi decay scheme.

labeled with the α-particle emitter, ^{211}At, has been injected into surgically created cavities in patients with malignant gliomas. This trial has demonstrated substantially better tumor control relative to ^{131}I-labeled 81C6 antibody (27).

Fifty to 60% of prostate cancer patients either present with or develop metastases in the course of their disease. Of those that metastasize, bone involvement occurs in >80% of cases (28). The unique propensity of prostatic epithelial cells to seed in the bone marrow and, in advanced disease, to disseminate as small (rapidly accessible) clusters, eventually invading the bone matrix to become skeletal metastases (29), forms a compelling rationale for investigating ^{213}Bi radioimmunotherapy against prostate cancer. In this study, spheroids of the prostate carcinoma cell line LNCaP-LN3 are used to investigate the potential efficacy and to optimize the use of ^{213}Bi-labeled anti-PSMA[4] antibody in targeting disseminated prostate cancer micrometastases.

MATERIALS AND METHODS

Cells. LNCaP-LN3 cells were provided by Drs. Curtis Pettaway and Isaiah Fidler of the M. D. Anderson Cancer Center. LNCaP cells of the LN3 subline exhibit a highly metastatic potential and produce all three prostatic biomarkers: prostatic acid phosphatase, prostate-specific antigen, and PSMA (30–32). The cells are hormonally responsive to testosterone, express high affinity to androgen receptors, and are tumorigenic in nude mice. Monolayer cultures were incubated in RPMI 1640 (Life Technologies, Inc., Grand Island, NY), supplemented with 10% fetal bovine serum (Gemini Bio-Products, Inc., Woodland, CA), 100 units/ml penicillin, and 100 μg/ml streptomycin. The cell cultures were kept at 37°C in a humidified 5% CO_2 and 95% air incubator.

Spheroids. Spheroids were initiated using the liquid overlay technique of Yuhas *et al.* (33). Details regarding LNCaP spheroid formation and characterization are described in Ballangrud *et al.* (17). Approximately 10^6 LNCaP-LN3 cells, obtained by trypsinization from growing monolayer cultures, were seeded into 100-mm dishes coated with a thin layer of 1% agar (Bacto Agar; Difco, Detroit, MI) with 15 ml of RPMI 1640, supplemented with 10% fetal bovine serum, 100 units/ml penicillin, and 100 μg/ml streptomycin. After 3–4 days, spheroids of approximate diameters 130 ± 20 μm and 180 ± 20 μm were selected under an inverted phase-contrast microscope with an ocular scale using an Eppendorf pipette. The selected spheroids were transferred to 35-mm bacteriological Petri dishes in 2 ml of medium for treatment.

Antibodies. The anti-PSMA antibody, J591, used in these experiments targets the external domain of PSMA (34). PSMA is expressed on the surface of the original LNCaP cells at a density of ~180,000 sites/cell (35, 36). Using a modified Scatchard analysis (37), an antigen site density for the LN3 subline of 130,000 sites/cell was measured. PSMA expression has also been found in tumor but not in normal vascular endothelium (34, 38). The anti-CD33 antibody, HuM195 (39, 40), was used as a nonspecific control.

^{213}Bi Labeling. The isothiocyanatobenzyl derivative of CHXA-DTPA (41–43) was used to chelate ^{213}Bi to the two antibodies. The radionuclide was available from an ^{225}Ac/^{213}Bi generator that was obtained from the Transuranic Research Institute (Karlsruhe, Germany) and the United States Department of Energy. Details regarding the ^{225}Ac/^{213}Bi generator and the chelation of ^{213}Bi to antibodies have been published previously (44, 45). The specific activity was 92.5 GBq/g (2.5 Ci/g) for both ^{213}Bi-J591 and ^{213}Bi-HuM195. Purity was 86% for ^{213}Bi-J591 and 98% for ^{213}Bi-HuM195.

Treatment Protocol. Spheroids were incubated with 0.9 and 1.8 MBq/ml ^{213}Bi on 10 μg/ml J591 (specific antibody) or HuM195 (hot control) for 15, 30, and 60 min and 24 h. Twenty-four spheroids were used in each experiment; after each incubation period, the spheroids were washed three times by suspension in fresh medium and placed in separate wells of a 24-well plate. Spheroids exposed to 10 μg/ml unlabeled J591 (cold control) and unexposed spheroids (control) were followed in the same manner. The medium in each well was replaced, and individual spheroid volume measurements were performed twice per week. An inverted phase microscope fitted with an ocular micrometer was used to determine the major and minor diameter d_{max} and d_{min}, respectively, of each spheroid. Spheroid volume was calculated as $V = \pi \cdot d_{max} \cdot d_{min}^2/6$. Volume monitoring was stopped once a spheroid had broken up or fragmented to individual cells or two to three cell clusters.

External Beam Irradiation. Spheroids were exposed to acute doses of 9 and 12 Gy external beam photon irradiation using a Cesium irradiator at a dose rate of 0.8 Gy/min (Cs-137 Model 68; JL Shepherd and Associates, Glendale, CA.). Volume measurements of 24 spheroids at each dose level were performed as described above.

Antibody Penetration. Spheroids of diameter 200 μm were incubated with 10 μg/ml FITC (F7250; Sigma Chemical Co., St. Louis, MO.)-conjugated J591 for 1, 2, 3, and 24 h and imaged by confocal microscope while still in the incubation medium. A 3-μm-thick optical section was acquired at the center of each spheroid. Five spheroids were imaged for each time point. Antibody concentration as a function of radial distance was obtained using MIAU, a software package developed in-house (46). Briefly, a circular erosion element was used to follow the exterior contour of each spheroid and delineate rings of 5-μm thickness. The average pixel intensity in each ring was converted to antibody concentration by calibration with the known external concentration of antibody. The antibody concentration as a function of distance from the rim of the spheroid was corrected for light attenuation. Confocal microscope images of the equator plane of spheroids derived from cells transfected with green fluorescent protein were used to determine an attenuation correction dependent on the diameter of the spheroid. The spatial distribution of antibody concentration after different incubation durations was then used to calculate the radial distribution of α emissions for dosimetry.

Dosimetry. The specific activity of the antibody was used to convert the radial distribution of antibody concentration to a radioactivity concentration that, in turn, was converted to a spatial distribution of ^{213}Bi decays by integrating the radioactivity concentration profiles over time. Absorbed dose in the spheroids was calculated by the Monte Carlo method described by Charlton (47). Monte Carlo simulations were used to provide the energy and direction of the α-particles originating from the ^{213}Bi decay distribution. The chord length of α-particle traversals through the spheroid was converted to energy deposition using the stopping powers data of Ziegler (48). This approach was also used to obtain the radial distribution of absorbed dose across the spheroid, as well as the mean absorbed dose over the whole spheroid volume; the former was obtained as the mean absorbed dose in 5-μm-thick shells.

Statistical Analysis. Differences in tumor volumes over time were analyzed using generalized estimating equation methodology (49). This method assesses differences in groups over time while accounting for the correlation within each spheroid. Approximately 25 time points were recorded on 24 spheroids/treatment strategy. Each treatment strategy was compared with the control group. In addition, ^{213}Bi-J591 for 24 h was compared with the 12-Gy group, and ^{213}Bi-J591 for 60 min was compared with the 9-Gy group. The P values were adjusted for multiple comparisons by the Bonferroni correction.

[4] The abbreviation used is: PSMA, prostate-specific membrane antigen.

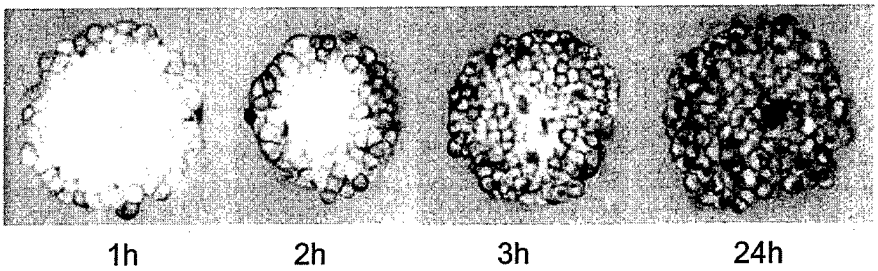

Fig. 2. Confocal microscopy slices through the equator of 200-μm-diameter LNCaP-LN3 spheroids after incubation with 10 μg/ml J591-FITC for 1, 2, 3, and 24 h.

RESULTS

Confocal microscope images of antibody penetration after 1, 2, 3, and 24 h incubation with J591-FITC are shown in Fig. 2. The images show tightly packed cells filling the spheroid volumes, with the FITC label as the darker areas. The antibody is capable of reaching the core after approximately four half-lives of ^{213}Bi. No binding was observed in spheroids incubated with the FITC-labeled control antibody, HuM195-FITC (not shown). The attenuation-corrected antibody concentration profiles for four different incubation periods are shown in Fig. 3 as a function of distance from the rim of the spheroids.

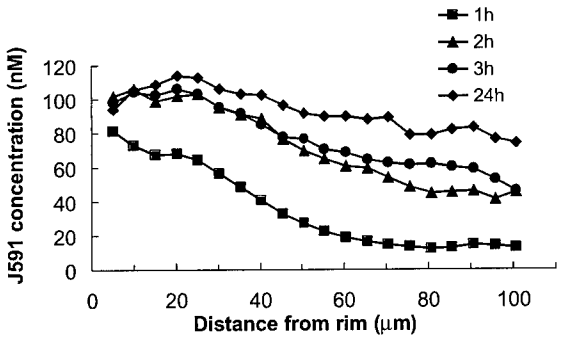

Fig. 3. Mean attenuation-corrected J591 concentration profiles in LNCaP-LN3 spheroids after 1-, 2-, 3-, and 24-h incubation with the antibody. Profiles were obtained by imaging five spheroids/time point.

Growth curves for individual spheroids of initial diameter 130 μm are shown in Fig. 4 after 24 h incubation with 0.9 and 1.8 MBq/ml ^{213}Bi-J591. Response after treatment with ^{213}Bi-HuM195 is shown as control. The growth curve in Fig. 4*d* was stopped at day 29 because of contamination of the culture plate. Spheroids irradiated with acute doses of 9 (Fig. 4*a*) and 12 Gy (Fig. 4*b*) external beam are shown in Fig. 5. Median spheroid volumes for spheroids incubated with 0.9 MBq/ml ^{213}Bi are compared with response after 9 and 12 Gy external beam photon irradiation in Fig. 6. The regrowth curves for all groups of treated spheroids were significantly different ($P < 0.001$) from the control spheroids, except for the group treated with unlabeled J591. No significant difference was found between spheroids incubated 24 h

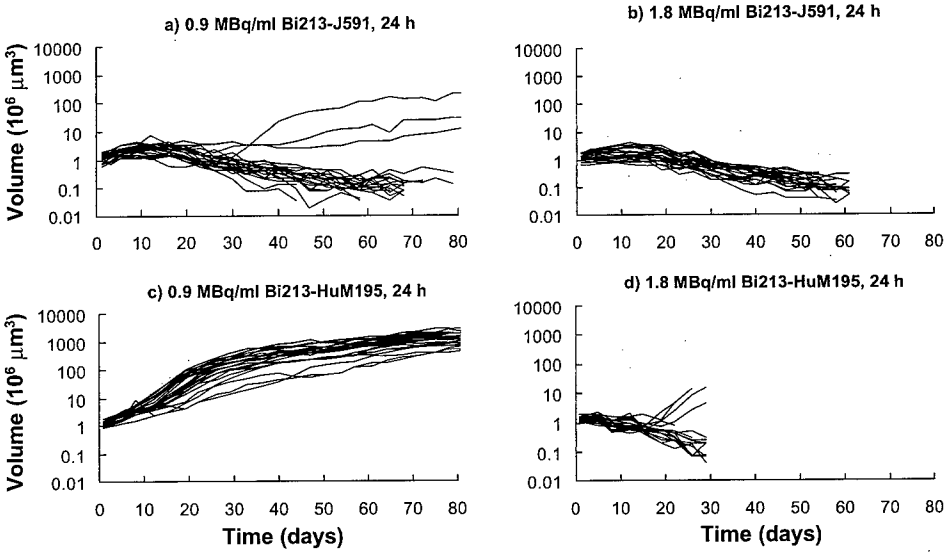

Fig. 4. Individual growth curves for spheroids with initial diameters of 130 ± 20 μm after a 24-h incubation with 0.9 MBq/ml ^{213}Bi-J591 (*a*), 1.8 MBq/ml ^{213}Bi-J591 (*b*), 0.9 MBq/ml ^{213}Bi-HuM195 (nonspecific antibody; *c*), and 1.8 MBq/ml ^{213}Bi-HuM195 (nonspecific antibody; *d*).

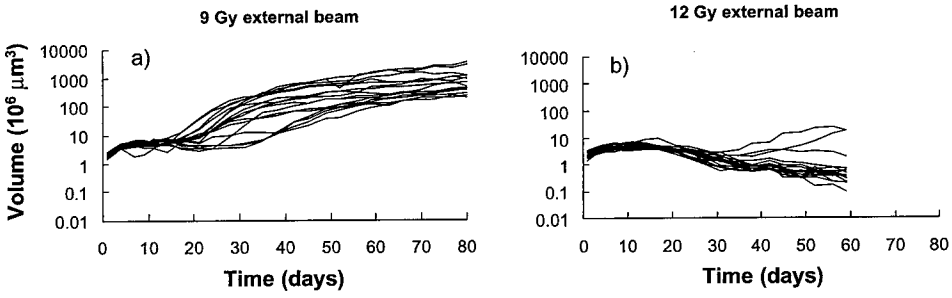

Fig. 5. Growth curves of individual spheroids after irradiation with an acute dose of 9 (*a*) and 12 (*b*) Gy external beam irradiation.

with 0.9 MBq/ml ^{213}Bi-J591 and those irradiated with 12 Gy external beam irradiation or between the spheroids incubated with ^{213}Bi-J591 for 60 min and those irradiated with 9 Gy external beam. The estimated mean absorbed dose to spheroids treated with 0.9 MBq/ml ^{213}Bi-J591 for 24 h was 3.7 Gy, suggesting a relative biological effectiveness factor of 3 over photon irradiation in this system.

To evaluate the impact of initial diameter on treatment response, growth curves for spheroids of initial median diameter of 180 μm were exposed to the same activity concentrations and incubation times as for the 130-μm-diameter spheroids. Growth curves for 180-μm-diameter spheroids are shown in Fig. 7. Monte Carlo-derived spatial dose distributions for 130- and 180-μm-diameter spheroids after treatment with 0.9 and 1.8 MBq/ml ^{213}Bi-J591 and HuM195 are shown in Fig. 8. Mean absorbed dose and spheroid fragmentation are summarized in Tables 1 and 2.

Light microscope images of one spheroid fragmenting (Fig. 9*a*), and one spheroid regrowing after 24 h incubation with 0.9 MBq/ml ^{213}Bi-J591 (Fig. 9*b*), and a ^{213}Bi-HuM195 treated spheroid (Fig. 9*c*) are shown. Four days after treatment, a 30–40-μm shell of shedding cells is observed in the spheroids treated with the specific antibody.

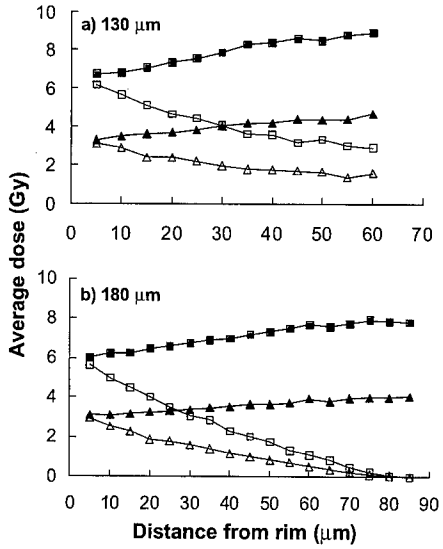

Fig. 8. Absorbed dose distribution for 130- and 180-μm spheroids treated with 0.9 MBq/ml ^{213}Bi-J591 (▲) and HuM195 (△), and 1.8 MBq/ml ^{213}Bi-J591 (■) and HuM195 (□).

DISCUSSION

Progression of prostate cancer is characterized by the dissemination of malignant prostatic epithelial cells and small clusters in the marrow. In advanced disease, such clusters remain small in size but increase in frequency throughout the marrow and skeleton (28). The extravascular space of bone marrow is rapidly accessible by i.v.-administered antibodies (39, 50, 51). Therefore, use of the spheroid model to examine α-emitter radioimmunotherapy of such metastases is particularly appropriate. This analysis suggests that treatment efficacy will critically depend upon the time at which therapy is implemented relative to the time course of metastatic dissemination. A treatment strategy in which the α-emitter-labeled antibody is used to target disseminated micrometastatic deposits in the vasculature or bone marrow of prostate cancer patients when a prostate-specific

Table 1 *Average absorbed dose estimates to spheroids*

	Absorbed dose (Gy)			
	130-μm-diameter spheroid		180-μm-diameter spheroid	
Treatment group	Specific	Nonspecific	Specific	Nonspecific
0.9 MBq/ml ^{213}Bi, 24 h	3.7	2.5	3.3	1.9
1.8 MBq/ml ^{213}Bi, 24 h	7.3	5.0	6.6	3.7

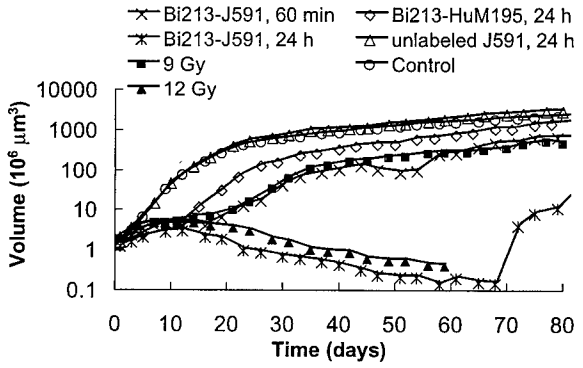

Fig. 6. Median spheroid volumes for spheroids incubated with 0.9 MBq/ml ^{213}Bi compared with response after 9 and 12 Gy external beam photon irradiation.

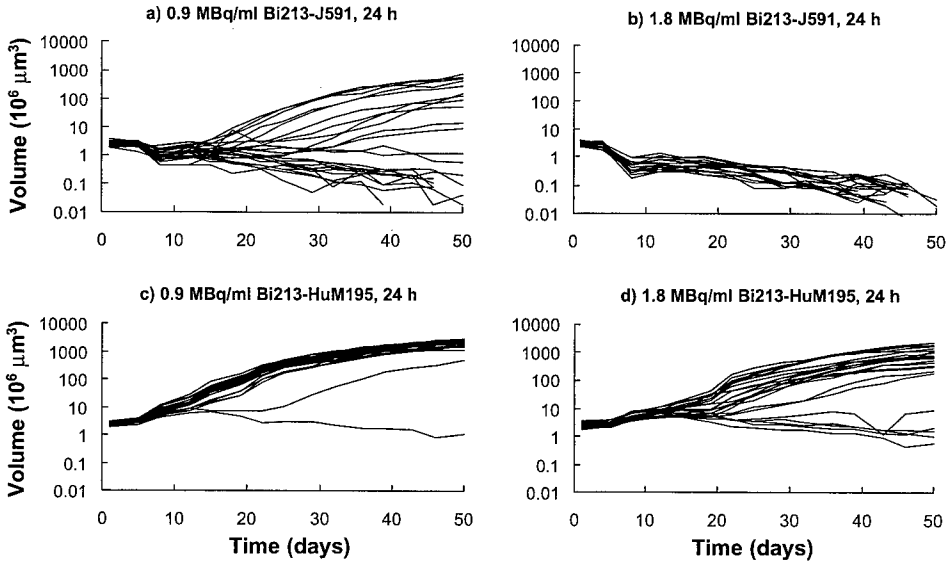

Fig. 7. Individual growth curves for spheroids with initial diameters 180 ± 20 μm after a 24-h incubation with 0.9 MBq/ml ^{213}Bi-J591 (*a*), 1.8 MBq/ml ^{213}Bi-J591 (*b*), 0.9 MBq/ml ^{213}Bi-HuM195 (nonspecific antibody; *c*), and 1.8 MBq/ml ^{213}Bi-HuM195 (nonspecific antibody; *d*).

Table 2 *Spheroid fragmentation (24 spheroids initially in each group)*

	No. of intact spheroids remaining			
	130-μm-diameter spheroid		180-μm-diameter spheroid	
Treatment group	Specific	Nonspecific	Specific	Nonspecific
0.9 MBq/ml ^{213}Bi, 24 h	3	24	10	23
1.8 MBq/ml ^{213}Bi, 24 h	0	n/a	0	19

antigen recurrence is first observed may reduce metastatic spread. Alternatively, a multi-injection treatment approach in which the interval between treatment is chosen so as to shift, with each successive treatment, the size distribution of micrometastases toward smaller diameter clusters is also likely to be effective. Longer-lived, α-particle-emitting radionuclides such as ^{211}At (half-life, 7.2 h; Ref. 52) and ^{225}Ac (half-life, 10 days; Ref. 53) may also provide an advantage if their toxicity is acceptable. Because of their longer half-life, these radionuclides are less susceptible to loss of activity because of the slow antibody penetration kinetics seen in micrometastases.

Extrapolation of the experimental conditions used in this study to a human administration assuming antibodies are initially confined to a vascular and extracellular fluid volume of 3.8 liters (plasma volume plus extracellular fluid of liver, spleen, and marrow; Ref. 54), corresponds to an i.v. injection of 3.4 GBq ^{213}Bi on 38 mg of antibody. In patients with leukemia, wherein localization of radiolabeled antibody occurred primarily in the marrow, 2.6 GBq of ^{213}Bi were administered with no evidence of dose-limiting toxicity. Furthermore, the hematological toxicity observed was not qualitatively different from that obtained in a similar population of patients treated with a β-emitter conjugated to the same antibody (55).

Fig. 2 shows that at an antibody concentration of 10 μg/ml, corresponding to 38 mg of antibody in a human antibody penetration is relatively slow, given the short half-life of ^{213}Bi. By 2 h, 76% of all ^{213}Bi decays have already occurred. As shown in Fig. 2, complete penetration of spheroids by antibody is not achieved prior to 3 h. The 81-μm range of the emitted αs compensates for this, however, and as shown in the growth delay curves, a clinically achievable activity concentration yields substantial spheroid volume reduction. However, as demonstrated by the response of 180-μm-diameter spheroids (Fig. 7) relative to the 130-μm-diameter spheroids (Fig. 4), the size distribution of micrometastases will have a critical impact on the efficacy of the treatment approach outlined above.

In Fig. 4*a*, three spheroids appear to be nonresponsive. The volumes of these are still 10- to 100-fold lower in volume than the hot control growth curves shown in Fig. 4*c*. We have no definitive explanations for why these three spheroids did not undergo fragmentation. It is possible that they reflect a heterogeneity in antigen expression, possibly derived from a subpopulation of cells whose antigen density was lower than the typical expression density of the cell population overall. The results depicted in Fig. 4*d* reflect "overkill," *i.e.*, the activity concentration used is higher than the threshold value for avoiding "toxicity" (characterized by substantial fragmentation of spheroids treated by radiolabeled, nonspecific antibody). Although the response shown in Fig. 4*b* is excellent, it comes at the price of greater toxicity. This result is consistent with the dose calculations depicted in Fig. 8*a*, showing that the absorbed dose profile from the nonspecific antibody at the high concentration is greater for a significant portion of the spheroid volume than the dose delivered by the specific antibody at the lower activity concentration. The results suggest that for 130-μm-diameter tumor cell clusters, the optimal activity concentration for achieving a response lies between 0.9 and 1.8 MBq/ml ^{213}Bi.

In Fig. 6, the rise seen in the Bi-213-J591, 24-h curve after day 70 may be explained by examining Fig. 4. The rise beyond day 70 reflects the disaggregation of spheroids represented by most of the declining growth curves so that the median value beyond 70 days is after the rising growth curves. The rise in the median is sharper than any of the individual spheroid curves because the first post-70 day point is the average of the third and fourth curves (from the *top*), whereas the second and third point is obtained from the third curve. There is a fourth point, not shown on the plot at $d = 82$ that explains the apparent rise seen beyond day 79. This point is obtained from the second curve because spheroids corresponding to the two lower curves have disaggregated by day 82.

As shown in Fig. 8, the spatial distribution of absorbed dose throughout both 130- and 180-μm-diameter spheroids, treated with the specific antibody, is generally uniform with a 1.3–1.4-fold "cross-fire"-related increase in the absorbed dose near the center of the spheroids. The reduction in efficacy seen between the two spheroid sizes does not, therefore, arise because a portion of the larger spheroid volume remains unirradiated but rather is attributable to the increase in cell number that must be sterilized to achieve spheroid fragmentation. Approximately 600 cells make up 130-μm-diameter spheroids; the number doubles to 1200 cells for 180-μm-diameter spheroids. By convolving an α-particle radiosensitivity derived from LNCaP cells grown in monolayer with the mean absorbed dose in each 5-μm-thick shell, it is possible to estimate that ~4 of 600 cells may be expected

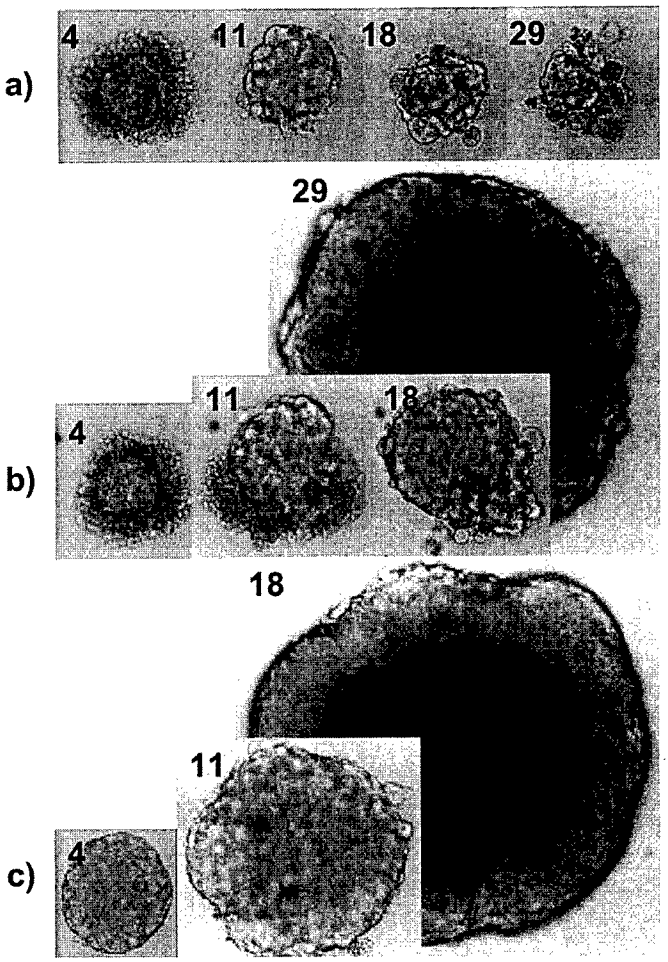

Fig. 9. Light microscope images on days 4, 11, 18, and 29 of two spheroids treated with 0.9 MBq/ml ^{213}Bi-J591, where one spheroid fragmented (*a*) and one spheroid experienced a growth delay but then finally continued to grow (*b*). *c*, a hot control is shown on days 4, 11, and 18.

to survive in smaller spheroids treated with 0.9 MBq/ml. The corresponding number of cells for the larger spheroids is 12 of 1200. The difference in absolute number of cells remaining is likely to be responsible for the observed differences in treatment efficacy. In 180-μm-diameter spheroids treated with the higher, 1.8 MBq/ml exposure, the number of cells expected to survive is 0.17. The much lower cell survival expected in this case is consistent with the results shown on Table 2, wherein all 24 of the larger spheroids fragmented after a 1.8 MBq/ml exposure. It is important to recognize that the radiosensitivity of cells in spheroid culture *versus* monolayer culture differs for low linear energy transfer emissions (56) and may also differ for α-particles (19). Nevertheless, the analysis demonstrates that the difference in response between the 130- *versus* the 180-μm-diameter spheroids is not a result of diminished absorbed dose but rather may be explained on basic radiobiological grounds (57).

The radial absorbed dose distributions for spheroids treated with the nonspecific antibody suggest that the differences in fragmentation arise, in this case, in part because the 81-μm range of Bi-213 α-particle emissions is insufficient to reach the center of the larger spheroids. Correspondingly, no dose is delivered to the center of 180-μm-diameter spheroids treated with either 0.9 or 1.8 MBq/ml nonspecific antibody.

Comparing the median volume reduction curves of nonspecific and specific antibody (Fig. 6), a 10–15-day delay may be anticipated before a differential therapeutic effect is seen. The images in Fig. 9, however, suggest that this is a result of cell swelling prior to lysis and elimination (see Fig. 9*a,* day 4 *versus* day 11).

Bone involvement in prostate cancer is the most common and potentially the most debilitating site of spread (28). Disruption of the process by which tumor cells seed the marrow to form skeletal metastases would be of great therapeutic value. The studies and analyses described in this work support the use of α-emitter radioimmunotherapy with ^{213}Bi and an anti-PSMA antibody in such a treatment strategy. Animal studies (21) and results from a clinical trial in patients with leukemia (55) suggest that the toxicity of such an approach will not be prohibitive.

ACKNOWLEDGMENTS

Confocal microscopy imaging was performed in collaboration with Dr. Katia Manova, director of the Molecular Cytology Core Facility, Memorial Sloan-Kettering Cancer Center. Cells expressing green fluorescent protein were kindly provided by Drs. Steven Larson and Bipin Mehta of the Nuclear Medicine Research Laboratory, Sloan-Kettering Institute. ^{225}Ac for ^{213}Bi generation was provided by PharmActinium, Inc., Chevy Chase, MD; The Institute for Transuranic Elements, Karlsruhe, Germany; and the Department of Energy, Isotopes Production, and Distribution.

REFERENCES

1. Kaminski, M. S., Zasadny, K. R., Francis, I. R., Milik, A. W., Ross, C. W., Moon, S. D., Crawford, S. M., Burgess, J. M., Petry, N. A., Butchko, G. M., *et al.* Radioimmunotherapy of B-cell lymphoma with [^{131}I]anti-B1 (anti-CD20) antibody. N. Engl. J. Med., *329:* 459–465, 1993.
2. Press, O. W., Eary, J. F., Appelbaum, F. R., Martin, P. J., Badger, C. C., Nelp, W. B., Glenn, S., Butchko, G., Fisher, D., Porter, B., *et al.* Radiolabeled-antibody therapy of B-cell lymphoma with autologous bone marrow support. N. Engl. J. Med., *329:* 1219–1224, 1993.
3. Witzig, T. E., White, C. A., Wiseman, G. A., Gordon, L. I., Emmanouilides, C., Raubitschek, A., Janakiraman, N., Gutheil, J., Schilder, R. J., Spies, S., Silverman, D. H., Parker, E., and Grillo-Lopez, A. J. Phase I/II trial of IDEC-Y2B8 radioimmunotherapy for treatment of relapsed or refractory CD20(+) B-cell non-Hodgkin's lymphoma. J. Clin. Oncol., *17:* 3793–3803, 1999.
4. Gerlowski, L. E., and Jain, R. K. Microvascular permeability of normal and neoplastic tissues. Microvasc. Res., *31:* 288–305, 1986.
5. Dvorak, H. F., Nagy, J. A., Dvorak, J. T., and Dvorak, A. M. Identification and characterization of the blood vessels of solid tumors that are leaky to circulating macromolecules. Am. J. Pathol., *133:* 95–109, 1988.
6. Jain, R. K., and Baxter, L. T. Mechanisms of heterogeneous distribution of monoclonal antibodies and other macromolecules in tumors: significance of elevated interstitial pressure. Cancer Res., *48:* 7022–7032, 1988.
7. Clauss, M. A., and Jain, R. K. Interstitial transport of rabbit and sheep antibodies in normal and neoplastic tissues. Cancer Res., *50:* 3487–3492, 1990.
8. Fujimori, K., Covell, D. G., Fletcher, J. E., and Weinstein, J. N. A modeling analysis of monoclonal antibody percolation through tumors: a binding-site barrier. J. Nucl. Med., *31:* 1191–1198, 1990.
9. Sgouros, G. Plasmapheresis in radioimmunotherapy of micrometastases: a mathematical modeling and dosimetrical analysis. J. Nucl. Med., *33:* 2167–2179, 1992.
10. Macklis, R. M., Kinsey, B. M., Kassis, A. I., Ferrara, J. L., Atcher, R. W., Hines, J. J., Coleman, C. N., Adelstein, S. J., and Burakoff, S. J. Radioimmunotherapy with α-particle-emitting immunoconjugates. Science (Washington DC), *240:* 1024–1026, 1988.
11. Humm, J. L., and Chin, L. M. A model of cell inactivation by α-particle internal emitters. Radiat. Res., *134:* 143–150, 1993.
12. Sutherland, R. M. Cell and environment interactions in tumor microregions: the multicell spheroid model. Science (Washington DC), *240:* 177–184, 1988.
13. Walker, K. A., Murray, T., Hilditch, T. E., Wheldon, T. E., Gregor, A., and Hann, I. M. A tumor spheroid model for antibody-targeted therapy of micrometastases. Br. J. Cancer, *58:* 13–16, 1988.
14. Kwok, C. S., Crivici, A., MacGregor, W. D., and Unger, M. W. Optimization of radioimmunotherapy using human malignant melanoma multicell spheroids as a model. Cancer Res., *49:* 3276–3281, 1989.
15. Bardies, M., Thedrez, P., Gestin, J. F., Marcille, B. M., Guerreau, D., Faivre-Chauvet, A., Mahe, M., Sai-Maurel, C., and Chatal, J. F. Use of multi-cell spheroids of ovarian carcinoma as an intraperitoneal radio-immunotherapy model: uptake, retention kinetics, and dosimetric evaluation. Int. J. Cancer, *50:* 984–991, 1992.
16. Essand, M., Nilsson, S., and Carlsson, J. Growth of prostatic cancer cells, DU 145, as multicellular spheroids and effects of estramustine. Anticancer Res., *13:* 1261–1268, 1993.
17. Ballangrud, A. M., Yang, W. H., Dnistrian, A., Lampen, N. M., and Sgouros, G. Growth and characterization of LNCaP prostate cancer cell spheroids. Clin. Cancer Res., *5:* 3171s–3176s, 1999.
18. Langmuir, V. K., McGann, J. K., Buchegger, F., and Sutherland, R. M. ^{131}I-anticarcinoembryonic antigen therapy of LS174T human colon adenocarcinoma spheroids. Cancer Res., *49:* 3401–3406, 1989.
19. Kennel, S. J., Stabin, M., Roeske, J. C., Foote, L. J., Lankford, P. K., Terzaghi-Howe, M., Patterson, H., Barkenbus, J., Popp, D. M., Boll, R., and Mirzadeh, S. Radiotoxicity of bismuth-213 bound to membranes of monolayer and spheroid cultures of tumor cells. Radiat. Res., *151:* 244–256, 1999.
20. Behr, T. M., Behe, M., Stabin, M. G., Wehrmann, E., Apostolidis, C., Molinet, R., Strutz, F., Fayyazi, A., Wieland, E., Gratz, S., Koch, L., Goldenberg, D. M., and Becker, W. High-linear energy transfer (LET) α *versus* low-LET β emitters in radioimmunotherapy of solid tumors: therapeutic efficacy and dose-limiting toxicity of 213Bi- *versus* 90Y-labeled CO17–1A Fab′ fragments in a human colonic cancer model. Cancer Res., *59:* 2635–2643, 1999.
21. Behr, T. M., Sgouros, G., Stabin, M. G., Behe, M., Angerstein, C., Blumenthal, R. D., Apostolidis, C., Molinet, R., Sharkey, R. M., Koch, L., Goldenberg, D. M., and Becker, W. Studies on the red marrow dosimetry in radioimmunotherapy: an experimental investigation of factors influencing the radiation-induced myelotoxicity in therapy with β-, Auger/conversion electron-, or α-emitters. Clin. Cancer Res., *5:* 3031s–3043s, 1999.
22. Kennel, S. J., and Mirzadeh, S. Vascular targeted radioimmunotherapy with 213Bi–an α-particle emitter. Nucl. Med. Biol., *25:* 241–246, 1998.
23. Zalutsky, M. R., McLendon, R. E., Garg, P. K., Archer, G. E., Schuster, J. M., and Bigner, D. D. Radioimmunotherapy of neoplastic meningitis in rats using an α-particle-emitting immunoconjugate. Cancer Res., *54:* 4719–4725, 1994.
24. Jurcic, J. G., McDevitt, M. R., Sgouros, G., Ballangrud, A. M., Finn, R. D., Geerlings, M. W., Humm, J. L., Molinet, R., Apostolidis, C., Larson, S. M., and Scheinberg, D. A. Targeted α-particle therapy for myeloid leukemias: a Phase I trial of bismuth-213-HuM195 (anti-CD33). Blood, *90:* 2245, 1997.
25. Sgouros, G., Ballangrud, A. M., Jurcic, J. G., McDevitt, M. R., Humm, J. L., Erdi, Y. E., Mehta, B. M., Finn, R. D., Larson, S. M., and Scheinberg, D. A. Pharmacokinetics and dosimetry of an α-particle emitter labeled antibody: 213Bi-HuM195 (anti-CD33) in patients with leukemia. J. Nucl. Med., *40:* 1935–1946, 1999.
26. Zalutsky, M. R., and Vaidyanathan, G. Astatine-211-labeled radiotherapeutics: an emerging approach to targeted α-particle radiotherapy. Curr. Pharm. Des., *6:* 1433–1455, 2000.
27. Zalutsky, M. R., Cokgor, I., Akabani, G., Friedman, H. S., Coleman, R. E., Friedman, A. H., McLendon, R. E., Reist, C. J., Pegram, C. M., Zhao, X. G., and Bigner, D. D. Phase I trial of α-particle-emitting astatine-211 labeled chimeric antitenascin antibody in recurrent malignant glioma patients. Proc. Am. Assoc. Cancer Res., *41:* 544, 2000.
28. Scher, H. I., and Cheung, L. W. K. Bone metastases: biology and therapy. Semin. Oncol., *21:* 630–656, 1994.
29. Haq, M., Goltzman, D., Tremblay, G., and Brodt, P. Rat prostate adenocarcinoma cells disseminate to bone and adhere preferentially to bone marrow-derived endothelial cells. Cancer Res., *52:* 4613–4619, 1992.
30. Pettaway, C. A., Pathak, S., Greene, G., Ramirez, E., Wilson, M. R., Killion, J. J., and Fidler, I. J. Selection of highly metastatic variants of different human prostatic carcinomas using orthotopic implantation in nude mice. Clin. Cancer Res., *2:* 1627–1636, 1996.
31. Horoszewicz, J. S., Leong, S. S., Kawinski, E., Karr, J. P., Rosenthal, H., Chu, T. M., Mirand, E. A., and Murphy, G. P. LNCaP model of human prostatic carcinoma. Cancer Res., *43:* 1809–1818, 1983.

32. Israeli, R. S., Powell, C. T., Corr, J. G., Fair, W. R., and Heston, W. D. Expression of the prostate-specific membrane antigen. Cancer Res., *54:* 1807–1811, 1994.
33. Yuhas, J. M., Li, A. P., Martinez, A. O., and Ladman, A. J. A simplified method for production and growth of multicellular tumor spheroids. Cancer Res., *37:* 3639–3643, 1977.
34. Liu, H., Moy, P., Kim, S., Xia, Y., Rajasekaran, A., Navarro, V., Knudsen, B., and Bander, N. H. Monoclonal antibodies to the extracellular domain of prostate-specific membrane antigen also react with tumor vascular endothelium. Cancer Res., *57:* 3629–3634, 1997.
35. Liu, H., Rajasekaran, A. K., Moy, P., Xia, Y., Kim, S., Navarro, V., Rahmati, R., and Bander, N. H. Constitutive and antibody-induced internalization of prostate-specific membrane antigen. Cancer Res., *58:* 4055–4060, 1998.
36. McDevitt, M. R., Barendswaard, E., Ma, D., Lai, L., Curcio, M. J., Sgouros, G., Ballangrud, A. M., Yang, W. H., Finn, R. D., Pelligreni, V., Geerlings, M. W., Jr., Brechbiel, M. W., Bander, N. H., and Scheinberg, D. A. An α-particle emitting bismuth-213 labeled antibody (J591) to the external domain of prostate specific membrane antigen. Cancer Res., *60:* 6095–6100, 2000.
37. Mason, D. W., and Williams, A. F. The kinetics of antibody binding to membrane antigens in solution and at the cell surface. Biochem. J., *187:* 1–20, 1980.
38. Silver, D. A., Pellicer, I., Fair, W. R., Heston, W. D., and Cordon-Cardo, C. Prostate-specific membrane antigen expression in normal and malignant human tissues. Clin. Cancer Res., *3:* 81–85, 1997.
39. Scheinberg, D. A., Tanimoto, M., McKenzie, S., Strife, A., Old, L. J., and Clarkson, B. D. Monoclonal antibody M195: a diagnostic marker for acute myelogenous leukemia. Leukemia (Baltimore), *3:* 440–445, 1989.
40. Tanimoto, M., Scheinberg, D. A., Cordon-Cardo, C., Huie, D., Clarkson, B. D., and Old, L. J. Restricted expression of an early myeloid and monocytic cell surface antigen defined by monoclonal antibody M195. Leukemia (Baltimore), *3:* 339–348, 1989.
41. Brechbiel, M. W., Pippin, C. G., McMury, T. J., Milenic, D., Roselli, M., Colcher, D., and Gansow, O. A. An effective chelating agent for labeling of monoclonal antibody with 212Bi for α-particle mediated radioimmunotherapy. J. Chem. Soc. Chem. Commun., *17:* 1169–1170, 1991.
42. Brechbiel, M. W., and Gansow, O. A. Synthesis of C-functionalized *trans*-cyclohexyldiethylenetriaminepenta-acetic acids for labeling of monoclonal antibodies with bismuth-212 α-particle emitter. J. Chem. Soc. Perkin Trans. I, *1:* 1173–1178, 1992.
43. Nikula, T. K., McDevitt, M. R., Finn, R. D., Wu, C., Kozak, R. W., Garmestani, K., Brechbiel, M. W., Curcio, M. J., Pippin, C. G., Tiffany-Jones, L., Geerlings, M. W., Sr., Apostolidis, C., Molinet, R., Geerlings, M. W., Jr., Gansow, O. A., and Scheinberg, D. A. α-Emitting bismuth cyclohexylbenzyl DTPA constructs of recombinant humanized anti-CD33 antibodies: pharmacokinetics, bioactivity, toxicity, and chemistry. J. Nucl. Med., *40:* 166–176, 1999.
44. McDevitt, M. R., Finn, R. D., Ma, D., Larson, S. M., and Scheinberg, D. A. Preparation of α-emitting 213Bi-labeled antibody constructs for clinical use. J. Nucl. Med., *40:* 1722–1727, 1999.
45. McDevitt, M. R., Finn, R. D., Sgouros, G., Ma, D., and Scheinberg, D. A. An 225Ac/213Bi generator system for therapeutic clinical applications: construction and operation. Appl. Radiat. Isot., *50:* 895–904, 1999.
46. Kolbert, K. S., Hamacher, K. A., Jurcic, J. G., Scheinberg, D. A., Larson, S. M., and Sgouros, G. Parametric images of antibody pharmacokinetics in Bi-213-HuM195 therapy of leukemia. J. Nucl. Med., *42:* 27–32, 2001.
47. Charlton, D. E. Radiation effects in spheroids of cells exposed to α emitters. Int. J. Radiat. Biol., *76:* 1555–1564, 2000.
48. Ziegler, J. Stopping and range of ions in matter (SRIM96). *In:* IBM Research. Yorktown, NY: IBM Corp., 1996.
49. Zeger, S. L., and Liang, K. Y. Longitudinal data analysis for discrete and continuous outcomes. Biometrics, *42:* 121–130, 1986.
50. Sgouros, G., Graham, M. C., Divgi, C. R., Larson, S. M., and Scheinberg, D. A. Modeling and dosimetry of monoclonal antibody M195 (anti-CD33) in acute myelogenous leukemia. J. Nucl. Med., *34:* 422–430, 1993.
51. Sgouros, G. Bone marrow dosimetry for radioimmunotherapy: theoretical considerations. J. Nucl. Med., *34:* 689–694, 1993.
52. Zalutsky, M. R., and Bigner, D. D. Radioimmunotherapy with α-particle-emitting radioimmunoconjugates. Acta Oncol., *35:* 373–379, 1996.
53. McDevitt, M. R., Sgouros, G., Finn, R. D., Humm, J. L., Jurcic, J. G., Larson, S. M., and Scheinberg, D. A. Radioimmunotherapy with α-emitting nuclides. Eur. J. Nucl. Med., *25:* 1341–1351, 1998.
54. Snyder, W. S., Cook, M. J., Nasset, E. S., Karhausen, L. R., Howells, G. P., and Tipton, I. H. Report of the task group on reference man. *In:* ICRP Publication, Vol. 23. Elmsford, NY: International Commission on Radiological Protection, 1975.
55. Sgouros, G., Ballangrud, A. M., Jurcic, J. G., Panageas, K. S., McDevitt, M. R., Finn, R. D., Larson, S. M., and Scheinberg, D. A. β *versus* α-emitter dose-response analysis in patients. J. Nucl. Med., *41:* 82P, 2000.
56. Olive, P. L., and Durand, R. E. Drug and radiation resistance in spheroids: cell contact and kinetics. Cancer Metastasis Rev., *13:* 121–138, 1994.
57. O'Donoghue, J. A., Bardies, M., and Wheldon, T. E. Relationships between tumor size and curability for uniformly targeted therapy with β-emitting radionuclides. J. Nucl. Med., *36:* 1902–1909, 1995.